UNIVERSIDADE D
COIMBRA

João Filipe Santos Patrício

EFFECTS OF PENTOSE PATHWAY INHIBITION ON GLUCOSE METABOLISM IN CELL CULTURE MODELS OF CANCER USING STABLE ISOTOPE TRACERS AND NMR

VOLUME 1

Dissertação no âmbito da Dissertação em Bioquímica orientada pelo Professor Rui de Albuquerque Carvalho e o Doutor John Griffith Jones e apresentada ao Departamento de Ciência da Vida da Faculdade de Ciência e Tecnologia da Universidade de Coimbra.

Julho de 2022

Acknowledgements

Em primeito lugar gostaría de à Universidade de Coimbra, ao Departamento de Ciências de Vida por me terem propocionado todas as condições para poder efetuar este ciclo de estudo.
Um agradecimento ao CNC e à plataforma de UC-NMR da Universidade de Coimbra poder me terem dado as condições necessárias para a realização desta tese.
Aos meus supervisores, Professor Rui Carvalho e Dr. John Jones, por todos os conselhos e todo o apoio que me deram, não só nesta tese como ao longo deste ciclo de estudos. Sinto que parte da minha paixão pelo estudo do metabolismo, foi por ter o previlégio de aprender com as pessoas certas.
Aos meus colegas de laboratório, tanto no Intermediary Metabolism como no Metabolic NMR profiling, por todos os valiosos conselhos e toda a simpátia. Um agradecimento especial para a Bárbara por todos os ensinamento que me passou e à Mariana pela ajuda na realização dos ensaios de metabolômica, mas também por todas as conversas e debates .
Um agradecimento ao grupo MitoXT por ter providenciado as melhores condições para a realização de todos os ensaios biológicos. Um agradecimento especial ao Dr. José Teixeira que foi um terceiro orientador e por tods os conselhos e ensinamentos que me passou.
Um agradecimento à minha família, ao Rui, ao Ricardo, à Cátia, à Carlota, à avó Juvelina, à tia Ilda, à tia Teresa, à tia Leninha e todos os outros famíliares. E um pedido desculpa por todas as vezes que não os consegui visitar.
Um agradecimento especial à minha família “adotiva”, à Zeca, ao Alexandre e ao Edu por terem estado sempre lá em todas as ocasiões.
À minha mãe que sempre acreditou em mim e foi sempre a minha fã, mesmo quando as coisas não corriam bem.
Por fim, o agradecimento mawasespecial para a Andreia, a mulher que sempre me ouviu em primeiro lugar, nos bons e maus momentos, e que sempre me deu o apoio e a motivação para continuar a tentar “encontrar o meu lugar ao sol”. Já o disse na Licenciatura e digo agora também...nunca teria alcançado metade do que já alcancei sem o teu apoio.

Abstract

Hepatocellular carcinoma (HCC) accounted for around 4% of all cancer cases in 2020. This number was expected to increase in the future, given the continuing poor prognosis, especially for HCC cases secondary to non-alcoholic fatty liver disease. Therefore, there was a need to understand cancer physiology to better develop therapeutic approaches. In this sense, we aimed to assess pentose phosphate pathway (PPP) as a potential target, in part because of its role in the production NADPH, which studies have showed to have a pivotal role in both catabolism, anabolism and redox homeostasis.

HepG2 cell line cultured with glucose and glutamine was provided with [U-^{13}C]glucose, [U-^{2}H]glucose and unlabelled glutamine for 48 hours and studied either in the presence of two doses or absence of Polydatin, an inhibitor of glucose-6-phosphate dehydrogenase. Growth curves and protein expression were determined by SRB assay and Western blot, respectively, while the aqueous extracts were analysed by ^{1}H and ^{13}C NMR. Metabolic fluxes (Glycolytic and Non-Glycolytic Rates), as well as metabolites quantifications and proteins' expression levels associated with glucose metabolism was determined to provide insights into glucose metabolism. As for the redox state assessments, they were determined by the ratio lactate to alanine, and the expression levels of proteins associated with Redox response and cytoskeleton arrangements.

There was a decrease in growth with the increase in polydatin concentration. This reduction was accompanied by metabolic profile more glycolytic in higher concentrations of Polydatin (p-value < 0.05). Cells treated with higher concentration of polydatin experienced higher ^{13}C lactate (p-value < 0.01), tyrosine (p-value < 0.05), ^{13}C alanine (p-value < 0.05) levels in extracellular media compared to Control and lower concentration of Polydatin. In terms of intracellular media, higher levels of polydatin were associated with higher levels phosphocreatine to creatine ratio (p-value < 0.05) and IDH 2 expression (p-value < 0.01). The ratio of lactate to alanine was significantly higher with the highest concentrations of polydatin ($p < 0.01$) while the expression of thioredoxin (p-value < 0.0001), α-tubulin (p-value < 0.001) and actin (p-value < 0.01) were significantly lower.

By affecting PPP, there was a shift in the cellular redox state, rather than a shift in glucose metabolism, resulting in an increase in ROS activity, which will lead to a decrease in HCC cell growth and proliferation, supporting the strategy of targeting the PPP as a means of treating HCC.

Resumo

Carcinoma hepatocellular (CHC) representa certa de 4 % de todos os casos de cancro em 2020. Este número é esperado que aumente no futuro, dado o fraco prognostico, particularmente em casos CHC que tem progedido de doença de fígado gordo não alcolico. Desta forma, existe urgente necessidade em compreender melhor a patofisiologia do cancro, de forma a desenvolver melhores abordagens terapeuticas. Tenho isto em mente, neste trabalho que verificar a vias das pentoses phosphato com um potencial alvo terapeutico, em parte devido ao seu papel na produção de NADPH, que estudo demonstraram o seu papel crucial no catbolismo, anabolismo e controlo do estado redox da célula.

Linha celular HepG2 foi cultivado com glucose, metade [U-^{13}C]glucose e outra metade [U-^{2}H]glucose, e glutamina não marcada por 48 horas e estudada na ausência ou na presença de duas concentrações de Polidatina, um inibidor da glucose-6-phosphato dehidrogenase. Curvas de crescimento e expressão de proteína foram determinado pelo ensaio de SRB e Western blot, respetivamente, enquanto os meios e extratos aquosos foram ^{1}H RMN e o ultimo foi complementado com uma ^{13}C RMN. Fluxos metabólicos (Taxa de glicose e taxa de glicolise), assim como quantificação de metabolitos e nívewasde expressão de proteínas associadas ao metabolismo da glucose foram determinados de forma a termos um visão mawasampla do metabolismo da glucose. Quanto à determinação do estado redox da célula, este foi avaliado pelo ratio lactato/alanina, bem como pelos nívewasde expressão de proteínas associadas à reposta ao stress oxidativo e arranjo do citoesqueleto.

Com o aumento da concentração de Polidatina houve um redução do crescimento celular. Esta redução foi acompanhada por mudança para um perfil metabólico mawasglicolitico (valor-p < 0.05). As células tratadas com maiores concentrações de Polidatina também apresentaram maiores concentrações de ^{13}C lactato (valor-p < 0.01), tirosina (valor-p < 0.05), ^{13}C alanina (valor-p < 0.05) em meios extracelulweres, comparando a controlo e células com baixas concentrações de Polidatina. No extratos, elevados nívewasde Polidatina está associados com altos nívewasdo rácio fosfocreatina/creatina (valor-p < 0.05) e baixa expressão de IDH 2 (valor-p < 0.01). Com o aumento da concentração de Polidatina a células apresentaram rácio lactato/alanina significativamente elevado (valor-p < 0.01), enquanto os nívewasde expresão de tioredoxina (valor-p < 0.0001), α-tubulina (valor-p < 0.001), e actina (valor-p < 0.01) eram significativamente baixos.

Em suma, com a inibição da via das pentoses fosfato, existe um mudança no estado redox da célula, em vez de uma mudança no metabolismo da glucose, resultando numa aumento da atividade de espécies reativas de oxigénio, levando a um decrescimo do crescimento e

proliferação de CHC, suportando o papel da via das pentose fosfato com forma de tratamento para o CHC.

Contents

Acknowledgements.....II
Abstract..... IV
Resumo..... VI
List of abbreviations X
Introduction..... 1
Hepatocellular Carcinoma 3
Insights in Cancer Metabolism 6
Pentose Phosphate Pathway..... 7
Glycolysis and Krebs Cycle..... 9
NADPH: The metabolic playmaker in cancer research.....12
Nuclear Magnetic Resonance and Metabolic Analysis.....13
Thesis Plan.....17
Materials & Methods.....21
Materials and Reagents 23
Cell Cultures.....23
Cell harvest and extraction 24
Sulforhodamine B (SRB) assay.....24
Resazurin assay 24
Protein quantification 24
G6PD activity assay 25
Western Blot.....25
NMR analysis 26
Metabolic analysis.....26
Statistical analysis 28
Results.....29
Protocol Optimizations 31
Effect of polydatin on glucose metabolism 33
..... 41
Effect of polydatin on cellular redox homeostasis.....41
Discussion 43
Protocol Optimizations 45
Effects of Polydatin on glucose metabolism.....45
Effects of Polydatin on Redox homeostasis.....47

Conclusion 49
References 53
Appendix 61

List of abbreviations

HCC - Hepatocellular carcinoma

PPP - Pentose phosphate pathway

NADPH – Reduced form of nicotinamide adenosine dinucleotide phosphate

[U-^{13}C] – Glucose – Glucose uniformly labelled with ^{13}C

[U-^{2}H] – Glucose – Glucose uniformly labelled with ^{2}H

SRB – Sulforhodamine B

^{1}H NMR – Proton (hydrogen) nuclear magnetic resonance

^{13}C NMR – Carbon nuclear magnetic resonance

CHC – Carcinoma hepatocellular

WHO – World Health Organization

NAFLD – Non-alcoholic fatty liver disease

CT – Computed tomography

MRI – Magnetic resonance imaging

BCLC – Barcelona Clinic Liver Cancer Algorithm

ATP – Adenosine triphosphate

SD – Succinate dehydrogenase

FD – Fumarase

PDH – Prolyl hydroxylases

HIF – Hypoxia-inducing factors

IDH – Isocitrate dehydrogenase

DNL – *De novo* lipogenesis

Ras – Rat sarcoma virus

PI3K – Phosphatidylinositol 3-kinase

Akt – Ak strain transforming

mTOR – Mammalian target of rapamycin

mRNA – Messenger RNA

LDHA – Lactate dehydrogenase A

cAMP – Cycling adenosine monophosphate

CREB – Cycling adenosine monophosphate -response element binding protein

G6P – Glucose-6-phosphate

TKT – Transketolase

TALDO – Transaldolase

G6PD – Glucose-6-phosphate dehydrogenase

EMT – Epithelial-Mesenchymal Transition

G3P – Glyceraldehyde-3-phosphate

NADH – Reduced form of nicotinamide adenosine dinucleotide

TCA – Tricarboxylic acid cycle (alternative name to Krebs cycle)

HKII – Hexokinase II

PKM2 – Pyruvate kinase M2

ROS – Reactive oxygen species

TRX – Thioredoxin

HMGCR – 3-hydroxy-3-methylglutaryl-coenzyme A reductase

NMR – Nuclear Magnetic Resonance

I – Nuclear spin

ΔE – Difference in energy between these two states

B_o – Strength of the field

γ – Gyromagnetic ratio

N_α – Lower energy state

M_o – Macroscopic magnetization

FID – Free induction decay

SNR – Signal-to-noise ratio

PCA – Principal component analysis

PLS-DA – Partial least squares discriminant analysis

NOE – Nuclear Overhauser effect

FBS – Fetal bovine serum

PBS – Phosphate-Buffer solution

OD – Optic density

BCA – Bicinchoninic acid

RIPA – Radioimmunoprecipitation assay

PMSF – Phenylmethylsulphonyl fluoride

PIC – Protease Inhibitor Cocktail

PVDF - Polyvinylidene difluoride

SDS–PAGE – SDS–polyacrylamide

TBS-T – Transfer buffer solution with Tween

HRP – Horseradish peroxidase

LD50 – Lethal dose for 50% of a given population

SOD1 – Superoxide dismutase

TRxR – Thioredoxin reductase

Introduction

The World Health Organization defines cancer as a group of diseases that can start in tissues with active cell division and were characterized by uncontrolled cell growth and propagation, which can spread within the tissue of origin as well as invade other tissues in a process called metastasis. In 2020, it was reported more than 19 million new cases worldwide and almost 10 million deaths, and according to Global Cancer Observatory, this number will continue to grow and, by 2040, it is estimated that the incidence of cancer is going to be around 30 million with 16 million deaths. Therefore, there is now, more than ever, a necessity to understand cancer pathology further and better in order to adapt and develop therapies for prevention and remission. (1,2)

Hepatocellular Carcinoma

Hepatocellular Carcinoma (HCC) accounts for most liver primary cancers (75-90%) with 900,000 new cases in 2020, representing 4.7% of all cancer cases according to WHO. Over the same period, HCC accounted for 830,000 deaths, representing 8.3% of all deaths attributed to cancer, being the fourth most deadly in terms of mortality rate. Figure 1 shows the estimated crude incidence rate of liver cancer in 2020, with the highest rates in Asia and Western Countries. This is particularly interesting since there is a growing link between HCC, obesity, and related metabolic complications such as non-alcoholic fatty liver disease (NAFLD) and type 2 diabetes. Thus, 13.0-38.5% of all HCC cases were associated with NAFLD (3–5). The study of liver cancer has a high urgency given that by 2040, it is predicted that both incidence and mortality rates will be almost double that of 2020 (2).

In terms of diagnosis, HCC is normally detected by imaging techniques such as CT, MRI, ultrasonography or by biopsy, depending on the growth of the tumour itself. In patients with cirrhosis, there is a distinct pattern detectable in MRI or CT with a sensitivity of 60-80% and a specificity of 90%. In non-cirrhotic patients, early diagnosis is much more challenging because cancer imaging was most difficult in initial HCC stages. Finally, there is no recognized circulating biomarker or non-invasive liver test for early detection of HCC in subjects that were free of other liver diseases such as cirrhosis. Thus, there is an urgent need to develop such diagnostic approaches given that HCC incidence secondary to obesity and NAFLD is projected to steeply increase over the next few years in many parts of the world.(5–7)

HCC diagnosis can be divided into sub-groups depending on the tumour size, number of nodules and other morphological features and it has different treatment regimens depending on its sub-groups, according to the Barcelona Clinic Liver Cancer Algorithm (BCLC). The initial stage (BCLC stage 0) is very early stage or “small HCC”, where there isa small nodule ≤ 2 cm. In these cases, the therapeutical solution can include tumour ablation by heat or resection. The

second stage (BCLC stage A) is characterized by two morphological features. A patient can either have a solitary nodule with diameter > 2 cm or 2 to 3 nodules, each with a diameter < 2 cm. In this stage, the therapeutical solution is either tumour ablation, resection or liver transplantation. In the intermediate stage (BCLC stage B) there is multinodular morphology with all nodules exceeding 3 cm diameter. An HCC patient in this stage can be treated by a procedure called chemoembolization, where the local blood supply is blocked immediately after a chemotherapeutic agent is infused to the tumour region. From the intermediate stage, the prognosis evolves to a more advanced stage (BCLC stage C) where there is macrovascular invasion and metastasis to extrahepatic tissues. For this stage the treatment options involve systemic therapies. The terminal stage of HCC (BCLC stage D) is characterized by a non-transplantable HCC where there is no therapeutical solution, other than palliative care. Unlike the earlier stages, this terminal stage is associated with impaired liver function, which contributes to a very poor prognosis (5,7,8).

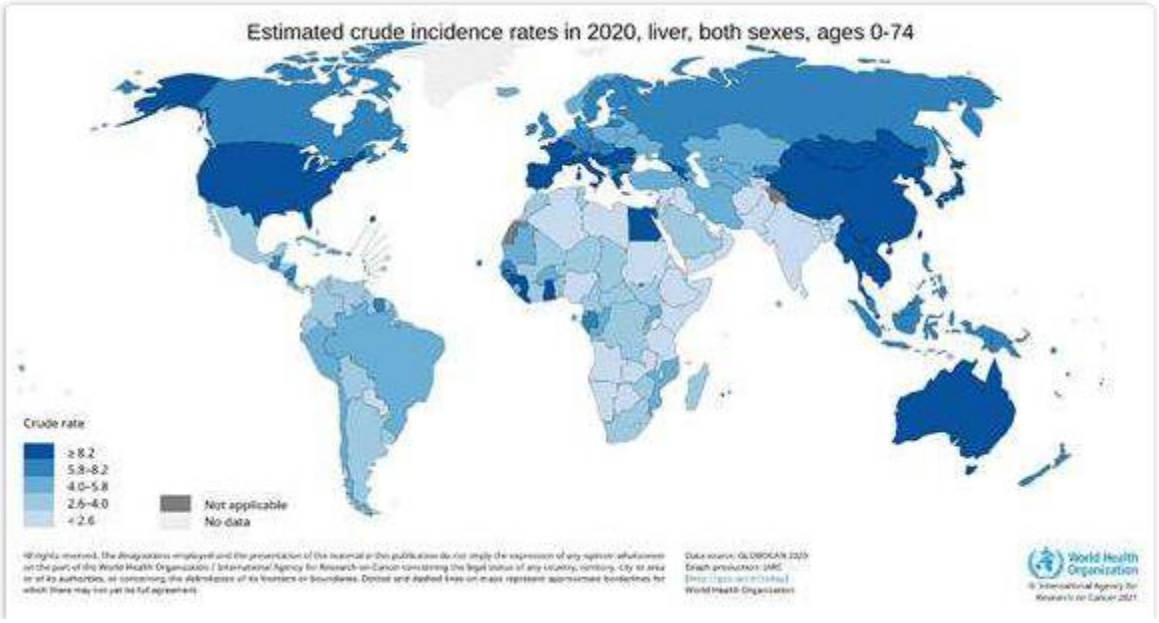

Figure 1 Global estimated crude incidence rates of liver cancer in 2020. Retrieved from (1).

HCC follows hepatic inflammation, fibrosis and aberrant hepatocyte regeneration which cause cirrhosis and induce a series of epigenetic and genetic alterations favouring tumour biogenesis, growth, and proliferation. Tumour cells also undergo profound alterations in intermediary metabolism, among which is an increased shift towards glycolysis as the main energy generating pathway even in the presence of high oxygen levels – as described over a century ago by Otto Warburg. Although overall less-energy efficient than aerobic respiration, this metabolic shift allows cancer cells to produce ATP at a faster rate than normal cells. Glucose

metabolism also generates intermediates such as lactate, amino acids and pentose phosphates to sustain biosynthesis. (6,8–13).

These changes were the effect of specific oncogenes and mutations in enzymes such as succinate dehydrogenase (SD) and fumarase (FD), that lead to the intracellular increase in succinate and fumarate, respectively. This in turn inhibits the activity of prolyl hydroxylases (PDH) on hypoxia-inducing factors (HIF), resulting in increased expression of specific oncogenes which inhibits oxidative Krebs cycle. Isocitrate dehydrogenase (IDH) mutants provide a shift in acetyl-CoA precursor for *de novo* lipogenesis (DNL), by allowing α-ketoglutarate, originating from glutamine, to be reductively carboxylated into isocitrate which on conversion to citrate yields acetyl-CoA via isocitrate lyase (9–12,14).

The Ras oncogene enhances glycolysis through the activation of glucose transporters and overexpression of glycolytic enzymes, hexokinase 2 and phosphofructokinase 1 via the PI3K/Akt pathway. Furthermore, this signalling pathway activates the mammalian target of rapamycin (mTOR) kinase. When activated, mTOR mediates biosynthesis via increased mRNA translation and ribosomal biosynthesises, as well as, increasing *de novo* lipogenesis and pentose phosphate pathway activities. In addition, mTOR also increases glycolytic flux though HIF translation. The MYC oncogene increases aerobic glycolysis by promoting the expression of lactate dehydrogenase A (LDHA), which interchanges pyruvate and lactate, thus promoting lactate production under normoxia. This action not only jeopardizes normal cell viability but also avails lactate as an alternative carbon precursor for both energy production and biosynthesis under conditions of low extracellular glucose concentrations. It is important to keep in mind that these oncogenes were both the result and cause of mutated enzymes and extracellular conditions, and it is the synergistic action of all these events that confer a higher resistance of cancer cells to alterations in physiological conditions (nutrient, O_2 availability and pH) compared to normal cells (9–11).

Cancer cells *per se* have outmatched those of the surrounding tissue in the ability to adapt to their immediate microenvironment. Essentially, changes in microenvironment - in part caused by the abnormal metabolic activity of the cancer cells themselves - involve altered nutrient availability, hypoxia, and extracellular acidity (11).

The microenvironment surrounding tumour cells is quite different when compared to that of surrounding healthy tissue with the cancer mass having more density and different blood vessel architecture due to angiogenesis. Moreover, because of the high glucose uptake by cancer cells, extracellular glucose becomes scarce. Several studies have reported that cancer cells can utilize alternative substrates for energy and biosynthetic precursors. These include lactate, ketone bodies, acetate, ammonia, and exogenous proteins (9,11,13).

Cancer cells were also faced with hypoxic conditions. Hypoxia is characterized by an oxygen percentage of 4-5%, unlike normoxia which have around 8% (21% for *in vitro* liver cells). In fact, hypoxia is the perfect example to elucidate the effects that environment have on cell metabolism and vice versa. In order to respond to this stress condition, cells have molecular mechanisms to sustain life, with hypoxia-inducible factor being among the most studied. HIF were a family of transcription factors, with two subunits, α and β, which sense the levels of O_2 and, when it is low, they shift central metabolism from aerobic to anaerobic respiration, among other things. Under physiological conditions, HIF were hydroxylated by PDH and marked by ubiquitin ligase complex for degradation. However, in cancer cells, due to the mutation in SD and FD, PDH is inhibited and there is stabilization of HIF activity, allowing glycolysis to be maintained even when O_2 levels were high (9,11,13,15–17).

Extracellular acidity associated with the overproduction of lactate is a common feature in cancer tissues and favours their growth and survival. Moreover, adaptation to acidosis is also shown for more aggressive and drug-resistant cancer cells. To respond to acidosis, cancer cells activate sterol regulatory element binding protein 2 (SREBP2), which induces cholesterol biosynthesis alongside overexpression of tumour-related genes (18). Interestingly, there is a reverse pH gradient between cancer and non-cancer cells. Cancer cells have intracellular pH around 7.2 while extracellular pH range from 6.7 to 7.1, whereas non-cancer cells' intracellular pH is, generally, around 7.2 while extracellular reaches 7.4. This reverse pH gradient is known to increase progression as well as metastasis, by inducing cAMP response to element binding protein (CREB) 1- p300/CREB binding protein interaction which promotes cell division. Moreover, recent studies have shown that destabilization in cancer cells' pH has proven to be an effective therapeutic strategy (11,18).

Given that HCC is one of the most aggressive and fastest growing tumours, it is not surprising that there is a close reliance on glucose metabolism, as mentioned before. Thus, targeting glycolysis and/or associated metabolic pathways could potentially be effective strategies for HCC therapy.

Insights in Cancer Metabolism

To better understand the role of altered metabolic activity in cancer pathology, firstly, one needs to understand the network of intermediary metabolic pathways, and how each pathway influences or is influenced by other pathways.

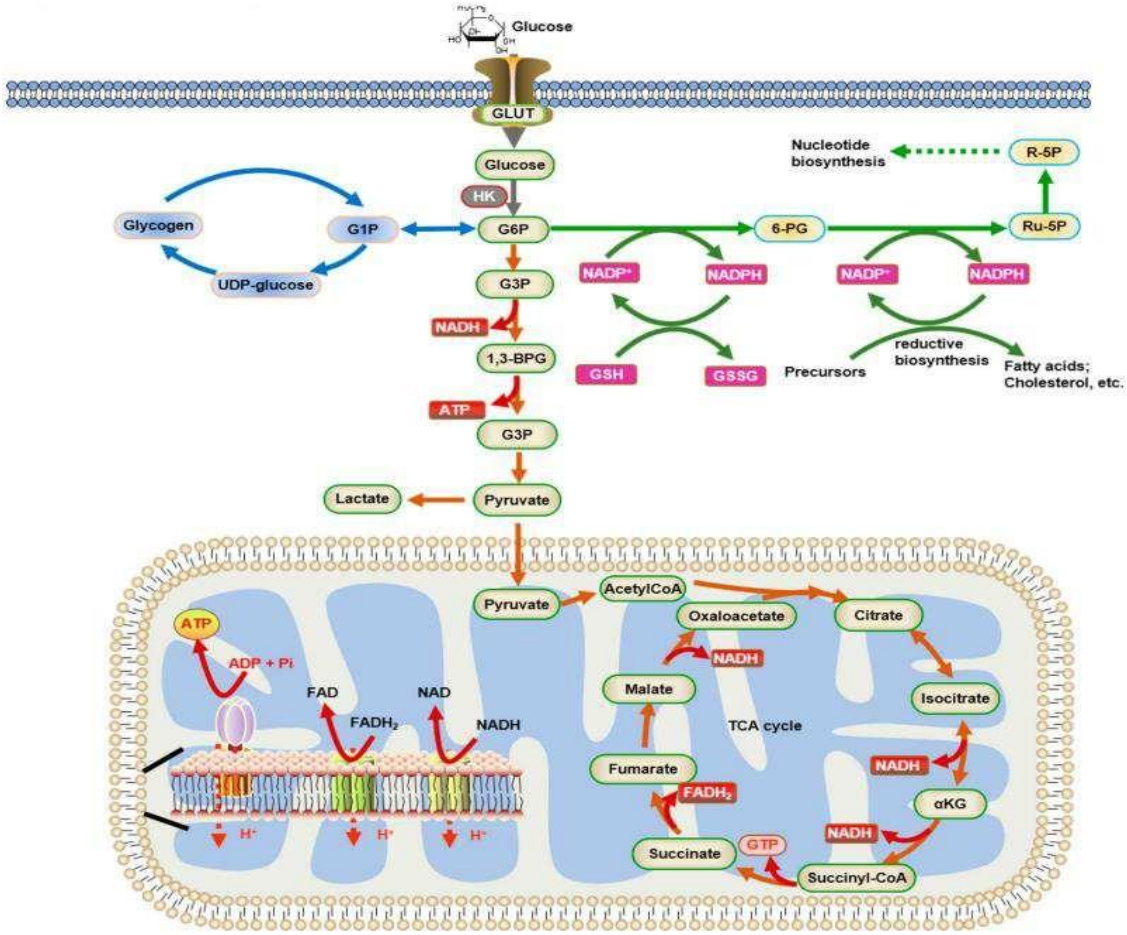

Figure 2 Principal glucose metabolic pathways. It was possible to see glycolysis, pentose phosphate pathway, glycogen production, Krebs cycle, and electron-transporter chain. Retrieved from (66).

Pentose Phosphate Pathway

The Pentose Phosphate Pathway, also known as hexose monophosphates hunt or phosphogluconate pathway, plays a pivotal role as both controller for cellular redox state and as a provider of building blocks for biosynthetic activities such as nucleotide synthesis.

This pathway starts after the phosphorylation of glucose into glucose-6-phosphate (G6P) of glycolysis, and it is then divided into two branches, the oxidative and non-oxidative. The oxidative branch is characterized, as the name indicates, by the multi-step oxidation of G6P to ribulose-5-phosphate, catalysed by glucose-6-phosphate dehydrogenase and 6-phosphogluconate dehydrogenase, with the production NADPH, for redox control and biosynthesis, as mentioned before. The non-oxidative branch is characterized by the rearrangement of ribose-5-phosphate into glycolytic intermediates, namely fructose-6-phosphate

and glyceraldehyde-3-phosphate to produce nucleotides and coenzymes. Two important enzymes that control the rate of this branch were transketolase (TKT) and transaldolase (TALDO), which catalyse the transfer of keto group from xylulose-5-phosphate to ribose-5-phosphate, forming sedohuptolose-7-phosphate and the removal of a three-carbon group from sedohuptolose-7-phosphate to form glyceralhyde-3-phosphate, respectively. Furthermore, this branch has been proven to be accelerated in cancer cells by the overexpression of TKT and TALDO, with the deficiency of the latter being able to prevent hepatocellular carcinoma (19–22).

In PPP, enzymes were subjected to allosteric control from their substrates, and to the crosstalk between oxidative and non-oxidative branches, as well as the crosstalk of other adjacent metabolic pathways, including glycolysis. For instance, if there is increased NADPH demand, the non-oxidative branch will increase the production of glycolytic intermediates to be converted to glucose-6-phosphate to replenish the oxidative branch. As such, there is a close relationship between PPP and glycolysis, given that they share common metabolites, while the components of each pathway contribute to regulating the activity of the other. Therefore, the study of PPP restraining as a therapeutical target for diseases, such as HCC is gaining more and more interest. The most studied enzyme in this pathway isglucose-6-phosphate dehydrogenase, which catalyses the oxidation of G6P into 6-phosphogluconolactone and NADPH and is the rate limiting step of the oxidative portion of the PPP. This enzyme is upregulated in most human cancers and correlates with a poor prognosis. It is upregulated by oncogenes like Ras, and by other promotors. PPP is also negatively regulated by oncosuppressors, such as p53. For the case of p53, this oncosuppressors acts directly, by restraining the glucose uptake and indirectly, by inhibiting phosphoglycerate mutase expression. Moreover, *Lu et al* found, in cell culture and in tissue samples of HCC, that overexpression of G6PD promotes migration and invasion through the activation of the epithelial to mesenchymal transition and its knockout could prevent migration and invasion and make the cells more susceptible to chemotherapeutics. Furthermore, the knockout of G6PD have also been showed to decrease cell viability in bladder cancer, resulting in the increase of ROS accumulation and suppression of Akt pathway. Recently, *Mele et al.* (21) have shown with in vitro study, in mammary cancer cells, that inhibition of G6PD by polydatin, a polyphenol derived from resveratrol (Fig. 2), could increase apoptosis by 50 % and inhibit invasion by 60 %. In addition, in vivo studies of tongue cancer with a dose of 100 mg/kg have induced tumour reduction of 30 % (19–25). Thus, polydatin isa potential therapeutic agent for preventing both cancer growth and proliferation.

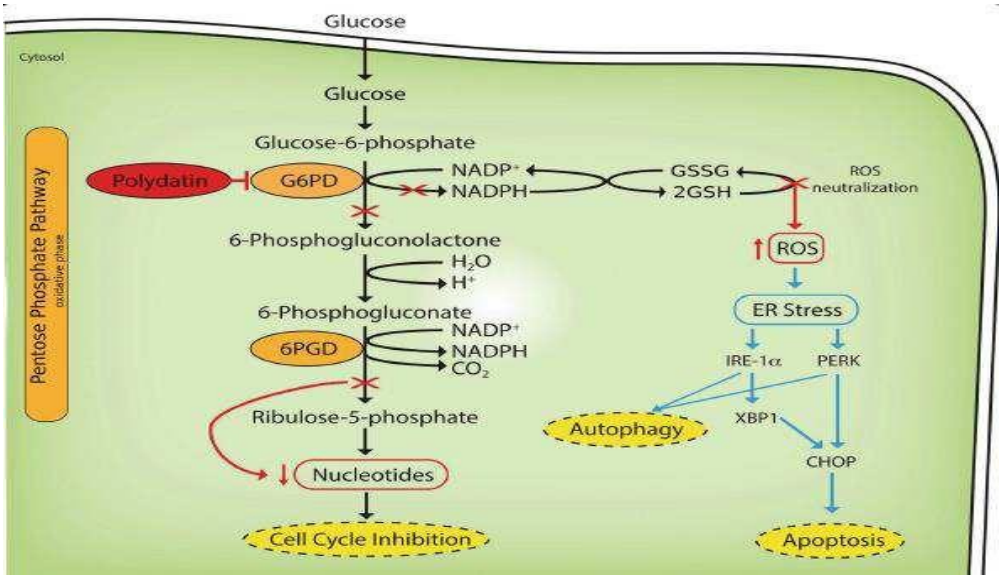

Figure 3 The mechanism of action of polydatin. As one can see, polydatin acts blocking G6PD activity, thus lower the nucleotide production as well as NADPH, making cancer cells more susceptible to ROS activity. Obtained from (21).

Glycolysis and Krebs Cycle

Glycolysis is the conversion of glucose into pyruvate in a ten enzyme-catalysed reaction, with the production of NADH for reducing equivalents and ATP for energy demands. Glycolytic intermediates also feed other metabolic pathways, such as fructose-6-phosphate and glyceraldehyde-3-phosphate for PPP, as mentioned before.

After uptake, glucose is immediately phosphorylated to G6P by hexokinase (or glucokinase in the liver). This reaction prevents the escape of glucose by adding a negatively charged group and is the first step of the preparatory stage of glycolysis. This preparatory stage consists of the conversion of one unit glucose (one six-carbon compound) into glyceraldehyde-3-phosphate and dihydroxyacetone phosphate (two three-carbon compounds), at the expense of two adenosine triphosphate (ATP). The beginning of the second phase of glycolysis starts with the isomerization of dihydroxyacetone phosphate into G3P and ends with dephosphorylation of phosphoenolpyruvate into pyruvate with the production NADH and ATP, as mentioned before (Fig.3). The pay-off phase consists of the oxidative phosphorylation of G3P into pyruvate with the production of two units of NADH and four units of ATP (for unit of glucose consumed). Glycolysis is regulated by several factors such as glycolytic enzymes, glucose uptake or/and hypoxia. Hexokinase, for example, controls the levels of glucose used by the cells. In most condition the most regulated enzyme in glycolysis is phosphofructokinase, which catalyse the irreversible production of fructose-1,6-biphosphate, step limiting reaction, which is regulated

by citrate, ATP and fatty acids and its inhibition cause negative feedback, inhibiting glycolysis (11,22,26,27).

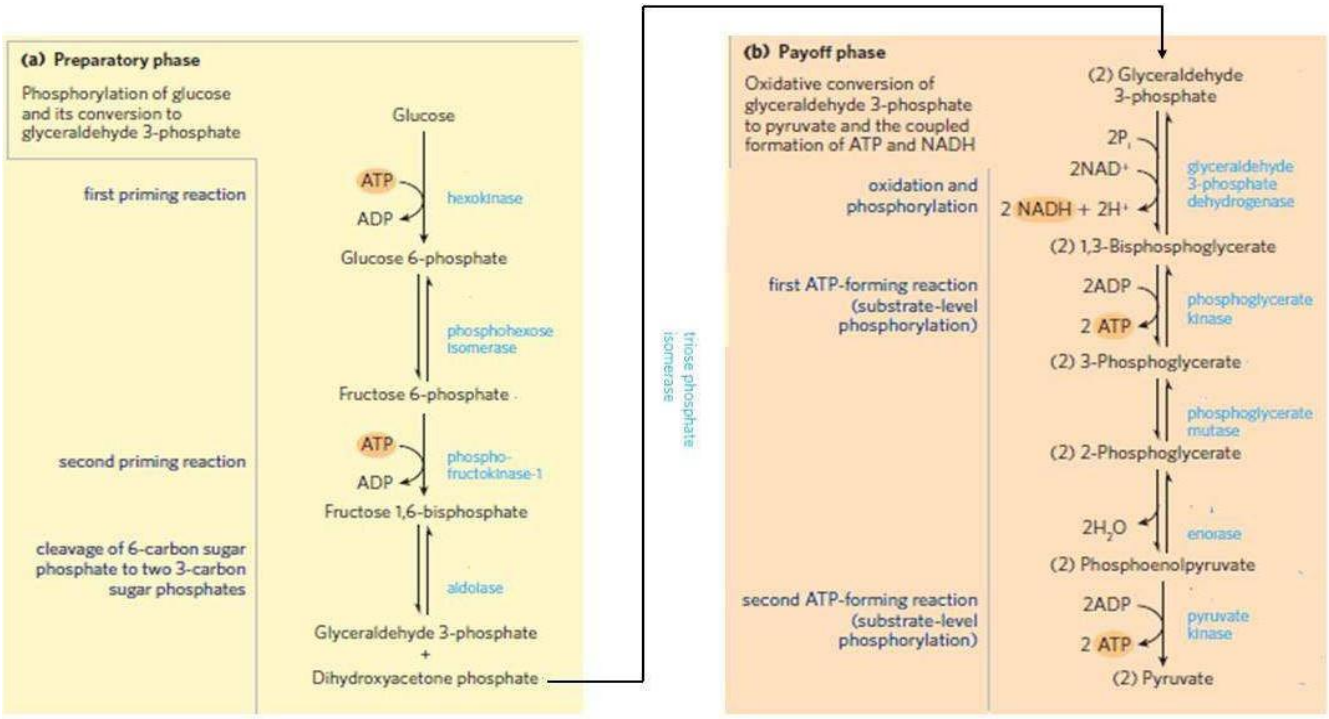

Figure 4 Glycolysis, separated into its two phases, preparatory and payoff phases. Adapted from (22).

Pyruvate is an important branch-point in central metabolism and therefore it is highly regulated. It can be reduced to lactate with the recovery of NADH, transaminated into alanine, carboxylated into oxaloacetate for replenishing of the Krebs cycle (anaplerosis) or decarboxylated into acetyl-CoA, to enter the oxidative Krebs cycle.

The Krebs cycle comprises 8 reactions that is a key hub of intermediary metabolism because of the production of reducing equivalents (NADH), as well as, precursors for *de novo* lipogenesis and biosynthesis of amino acids and sugars. The cycle starts with the synthesis of citrate from oxaloacetate and acetyl-CoA, which is then isomerized into isocitrate by aconitase. After this, isocitrate is oxidized to α-ketoglutarate by isocitrate dehydrogenase. In the presence of ^{13}C-enriched substrates, the rapid equilibrium between α-ketoglutarate and glutamate provides an important "magnifying glass" into Krebs cycle turnover and substrate selection via glutamate ^{13}C-isotopomer analysis. The next reaction is another oxidative decarboxylation by α-ketoglutarate dehydrogenase complex that converts α-ketoglutarate to succinyl-CoA. Succinyl-CoA is then converted to succinate by succinyl-CoA synthetase followed by dehydrogenation

into fumarate via succinate dehydrogenase. The ultimate step of the Krebs cycle involves oxidation of malate to oxaloacetate, catalysed by malate dehydrogenase (Fig. 4) (22,28).

A very important role of the Krebs cycle is a central hub of the metabolism. This means that Krebs cycle's intermediates were precursors for other metabolic pathways. For example, citrate for DNL, aspartate, from oxaloacetate for amino acid synthesis, glutamate, from α-ketoglutarate to redox response. Therefore, in order to fulfil both biosynthetic needs and oxidation of acetyl-CoA, the maintenance of intermediates pool sizes is vital. This maintenance is achieved via anaplerosis. Anaplerosis metabolic reactions that serves for replenish the Krebs cycle, besides the acetyl-CoA oxidation. Two examples of the anaplerotic reactions were the carboxylation of pyruvate to produce oxaloacetate via pyruvate carboxylation and the deamination of glutamine to glutamate and subsequently to α-ketoglutarate via glutaminase and glutamate dehydrogenase respectively. Given the importance of Krebs cycle and the crosstalk it showers with several metabolic pathways, (both anabolic and catabolic pathways) both anaplerosis and cataplerosis(which is the exportation of intermediates out of the Krebs cycle) regulate the intermediates pool's sizes depending on intracellular requirements. Furthermore, pyruvate carboxylation (by pyruvate carboxylase) appears as a good example of this tissue-specific anaplerosis, given that in the liver, an organ known for its biosynthetic role, is almost 10-fold higher than pyruvate oxidative decarboxylation (by pyruvate dehydrogenase), whereas in heart, a known oxidative organ, anaplerosis account for around 10% of the TCA flux (28).

As mentioned before, the regulation of both cataplerotic, anaplerotic and oxidative Krebs cycle were a key factor for the cellular viability. This is true for cancer cells, as well, with several enzymes from both glycolysis and Krebs cycle being upregulated, such as HKII, PKM2, or IDH2 support energy requirements and supply of biosynthetic precursors. Moreover, there is also an upregulation of glucose transporters which result in a higher glucose uptake and, subsequently decrease in extracellular glucose concentration a nutritional shift that favours cancer cells' capability of using alternative substrate, such as lactate, alanine, or glutamine, to fulfil cellular requirements. Besides energy and biosynthetic supply, both glycolysis and Krebs cycle have important roles in antioxidant defence, both by providing building blocks for antioxidant systems, such as glutamate for glutathione, and by providing reducing equivalents (NADPH) for regeneration of the reduced forms.

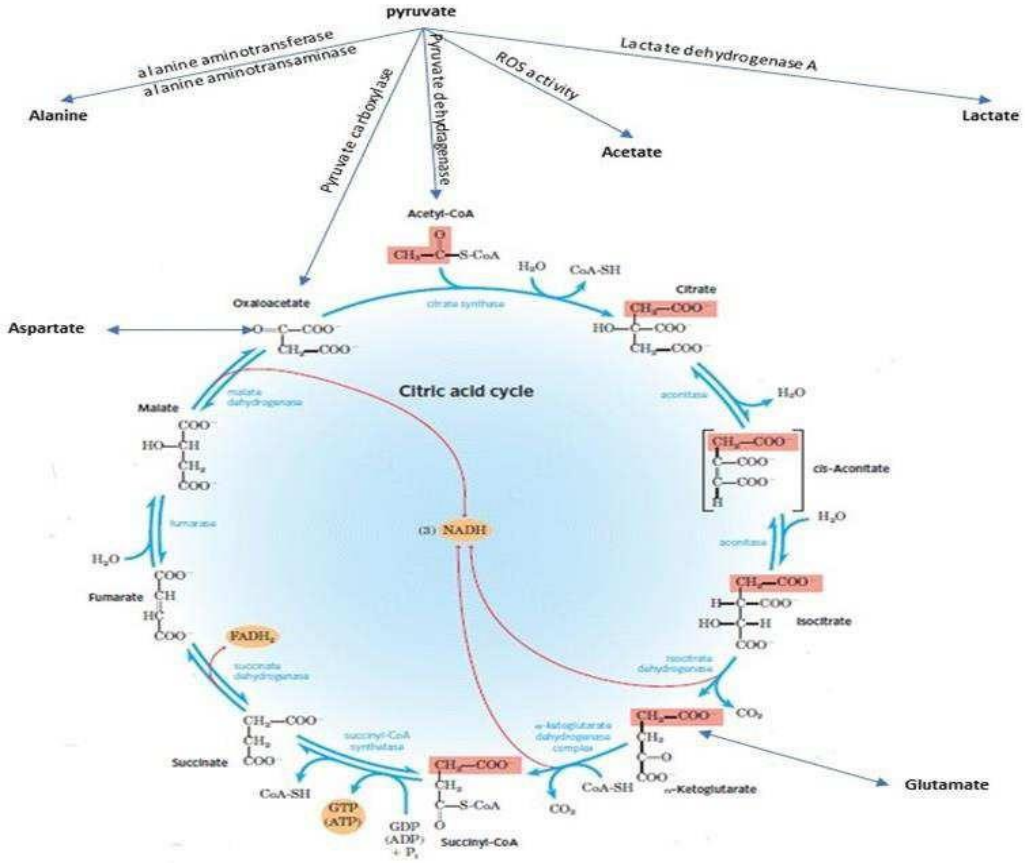

Figure 5 Schematic image illustrating the different cellular fates of pyruvate with emphasis on Krebs cycle (Citric acid cycle). Here was also illustrated example of both anaplerotic (carboxylation of pyruvate to oxaloacetate) and cataplerotic (amination of α-keto-glutarate in glutamate). Adapted from (22).

NADPH: The metabolic playmaker in cancer research

Nicotinamide adenosine dinucleotide phosphate is a coenzyme that act as an electron donor or acceptor, depending on whether it is in the reduced form (NADPH) or the oxidated form ($NADP^+$). As mentioned before, NADPH is key component of a variety of vital cellular processes, including control of cellular redox state and biosynthetic pathways.

In cancer cells, due to microenvironment conditions and because of therapies, there is an increased presence of ROS species. This is dangerous to a cell since it leads to DNA damage and cell death. To overcome ROS activity, cells have antioxidant systems that scavenge and neutralize ROS, one of which is the glutathione system, that uses NADPH as cofactor and an electron donor. Other example is the TRX system that uses NADPH to scavage ROS species and decrease DNA synthesis to prevent DNA mutation and apoptosis (29).

NADPH is also an essential cofactor for DNL, as well as a requirement for cholesterol synthesis, where it acts as reducing agent for 3-hydroxy-3-methylglutaryl-coenzyme A reductase (HMGCR) – the rate-limiting step in the cholesterol production; in folate metabolism, where it reduces dihydrofolate to tetrahydrofolate, in a reaction catalysed by dihydrofolate reductase (29–31).

With this wide functionality, it is extremely important to maintain NADPH homeostasis. NAPDH is produced from several pathways with PPP considered to account for the majority in many tissues. However, there other reactions that produce NADPH, such as NADP-malic enzyme, which converts malate into pyruvate; NADP-dependent isocitrate dehydrogenase (IDH1 and IDH2), folate-mediated serine catabolism, nicotinamide nucleotide transhydrogenase, which transfers a hydrogen from NADH to NADPH and accounts for around 45% of mitochondrial NADPH and NADH kinase, which produces NADPH by direct phosphorylation of NADH. The importance of NADPH in cancer cells is underlined by the fact that that several of these enzymes were overexpressed thereby boosting its bioavailability (9,20,29,32–37). Therefore, inhibiting NADPH formation is promising primary therapeutic target for cancer cells, as well as a complementary target to chemotherapeutics, since most mechanism of actions rely on ROS generating and control NADPH availability can increase effectiveness of such cancer therapeutics.

Nuclear Magnetic Resonance and Metabolic Analysis

Nuclear Magnetic Resonance (NMR) Spectroscopy is first described by Purcell and Bloch in 1946 and in subsequent decades has been developed into one of the most versatile and widely used analytical tools for characterizing molecular structure and stable isotope enrichment of biological material in part due to it being a non-destructive method with high reproducibility (38,39).

NMR Spectroscopy is based on several principles. First, most of nuclei have nuclear spin and this spin influences the magnetic moment of the nuclei as shown in Eq. 1. These proprieties were required for a certain nucleus (^{1}H, ^{13}C, ^{18}O) to appear in an NMR spectrum.

$$\mu = \gamma\sqrt{I(I+1)}\hbar \qquad (1)$$

By understanding Eq. 1, this means that if a nucleus has a nuclear spin (I) equal to 0, the magnetic momentum will be 0 and, therefore, it will not generate an NMR signal. This is the case for nuclei with an even number of protons and neutrons such as ^{12}C and ^{16}O. Another principle is when a collection of NMR active nuclei is placed in a static external magnetic field, in accordance to quantum mechanical selection rules, each nucleus either aligns with or against the field. The difference in energy between these two states, ΔE, is related to the strength of the field (B_o) and the gyromagnetic ratio (γ) – an intrinsic parameter related to the degree to which the nucleus interacts with the magnetic field - as shown in Eq. 2 (40).

$$\Delta E = \gamma\hbar B_o \qquad (2)$$

As expected, ΔE increases when the external magnetic field strength is increased. Also, for a given field strength, ΔE is higher for nuclei with high γ (for example ^{1}H or ^{19}F) compared with those of lower γ (for example ^{13}C or ^{2}H).

Under conditions of thermal equilibrium, the nuclei distribute between the two energy levels according to the Boltzmann distribution, given by Eq.3.

$$\frac{N_\beta}{N_\alpha} = 1 - \frac{\Delta E}{\kappa_B T} = 1 - \frac{\gamma \hbar B_o}{\kappa_B T} \qquad (3)$$

Even for the highest γ nuclei, ΔE is far smaller than $\kappa_B T$ therefore the populations of the two energy levels were almost equal. This is the reason behind one of the biggest limitations with this technique, which is its inherently lower sensitivity compared to other spectroscopic approaches such as UV-VIS spectroscopy (where the separation of energy levels were several orders of magnitude larger).

The small excess of nuclear spins in the lower energy state (N_α), results in a macroscopic magnetization of M_o, in an applied magnetic field, B_o (Fig. 3). Lastly, the resonance condition states that allowable transitions were those with ΔE corresponding to the Larmor frequency, which in turn is related to a quantum of energy (Eq. 4) (40).

$$\Delta E = h\nu_1 \qquad \nu_1 = \nu_L = \left|\frac{\gamma}{2\pi}\right| B_o \qquad (4)$$

Considering these principles, the basis of NMR methodology is applying a pulse of electromagnetic radiation to a sample on a static magnetic field, changing the M_o by exciting the excess population in N_α to move to N_β, and analysing the return to initial magnetization, through the Fourier transformation of the emitted radiation from the return to N_α, as free induction decay (FID) (40). Because the signal from the emitted radiation is extremely weak, the spectrometer collects and sums multiple FID to improve the signal-to-noise ratio (SNR).

The proton (^{1}H) has the highest γ of any non-radioactive nucleus and is therefore the most sensitive in terms of NMR detection. Almost all small and mobile biological molecules contain ^{1}H which generates sharp NMR signals, therefore ^{1}H NMR provides a rich source of information on metabolites. ^{1}H NMR metabolomics is a very useful tool in metabolic research. Its basis lies on metabolite identification, quantification, and comparison (by multivariate

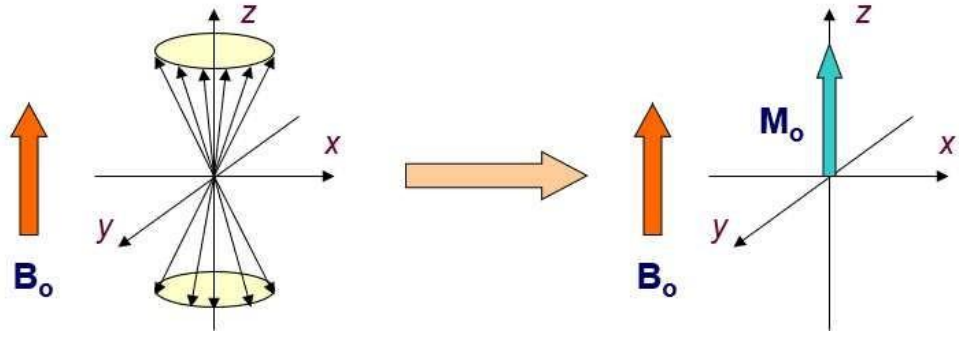

Figure 6 Scheme explain the principle of macroscopic Magnetization M_o.

statistical analysis) between different metabolic conditions. In many commercially available softwares (for example MetaboAnalyst) the comparison can be done, one of two ways, either by identify each metabolite, quantifying and compared the quantification of studied groups or by fragmentating the NMR spectra into to small intervals of spectra (or bins), comparing the bins between groups, followed by identification and quantification (41–43).

In terms of multivariate analysis, the most common analysis were principal component analysis (PCA) and partial least squares discriminant analysis (PLS-DA). PCA is an unsupervised method for data reduction in order to preserve and explain data variance. The characterization of PCA as an unsupervised method comes from the fact that PCA does not take into consideration the group distribution. PLS-DA is a supervised method for data reduction which creates a multivariate regression model for the studied group. There were two aspects to take into consideration in PLS-DA. First, being a supervised method, it inputs the group identity of the data set, which facilitates better separation of the data clusters. However, this feature can also contribute to overfitting of the model to the data thereby generating artificial separation of data clusters. Therefore, validation must be used to address this potential problem. The most common processes of validation were cross-validation and permutation. Cross validation is method used to determine the quality of the model and the result is described as quality parameters. The quality parameters most mentioned in metabolomics literature is R^2 which asses how good the model fit the data and Q^2 which describes how well the model predicts the data (for both parameters the highest value is 1). The other process of validation is permutation, which consist of analysing a data set, performing all possible permutations on our data set, and calculating the statistical test for every permutation. The output is usually represented as *p*-value (41,43).

The most abundant carbon isotope is the ^{12}C, although, it is not an NMR active nucleus, as mentioned before. Therefore, isotope must be used in order to assess this nucleus, present in all living organism, as for ^{1}H, although the latter is an NMR active nucleus. Initially, ^{14}C tracers were used in metabolic research due to its high sensibility and sensitivity. However, this isotope has been replaced due to fact its radioactivity and instability, rendering any long terms study in living organism complicated, beside the impossibility of combining multiple isotopes in the same living organism. In this sense of ^{13}C tracers appears as reliable and secure alternative, given the fact that this isotope is both stable and safe to use in human studies. Although these key advantages, ^{13}C have very low abundant in nature, 1.1%, which results in a signal around 10^{-4} relative to the sensitivity of ^{1}H. Beside this problem, ^{13}C has a γ that is about 25% of ^{1}H, because of higher mass of carbon nucleus. For ^{13}C NMR analysis, one key factor is the fact that the majority of ^{13}C were bound to one or more ^{1}H resulting in a splitting of the ^{13}C signal by

^{13}C-^{1}H coupling. This splitting typically does not provide additional structural information and decreases the SNR. Therefore, ^{13}C NMR spectra were typically acquired with ^{1}H-decoupling, a procedure that abolishes the signal splitting and also provides a significant enhancement of the decoupled signal via the nuclear Overhauser effect (NOE). This phenomenon is described as the perturbance of a nucleus splitting, i.e. ^{13}C, for the polarization transfer of the other nucleus, i.e. ^{1}H, resulting in a new splitting, in this example from 2 levels of energy for each nuclei to 4 levels (44,45).

It is now possible to obtain a wide array of precursor substrates including, glucose and glutamine, that were uniformly enriched to ~99% with ^{13}C (i.e. almost 100-fold higher than background). Metabolism of these substrates results in the ^{13}C enrichment of metabolic intermediates and products in excess of the background 1.1% level. Among other things, this level of excess ^{13}C-enrichment is related to how efficiently the ^{13}C-enriched substrate is utilized compared to endogenous ^{12}C precursors, and the degree of isotopic equilibration (i.e. replacement of pre-existing ^{12}C-metabolites within metabolite pools with the newly-formed ^{13}C-species). Thus, this approach potentially provides information on substrate preference as well as metabolic flux kinetics. On top of this, ^{13}C NMR also provides specific information on the position of ^{13}C-enrichment within a given metabolite carbon skeleton and whether or not the neighbouring carbons were enriched with ^{13}C. The basis for this is the splitting of ^{13}C signals by J-coupling with neighbouring ^{13}C nuclei. Moreover, these spin-coupled ^{13}C-signals were fully resolved from the background natural abundance ^{13}C singlet signals. This means that even very low excess ^{13}C-enrichments (0.5% or less) can be reliably resolved and quantified.

This highly specific resolution of multiple ^{13}C-enrichment patterns within metabolite carbon skeletons (also called ^{13}C-isotopomer analysis) allows the fate of ^{13}C to be precisely followed through complex metabolic networks such as the Krebs cycle with anaplerosis and pyruvate cycling (46,47), PPP (48) and DNL (49). These data can then be utilized by detailed and realistic metabolic flux models to provide comprehensive and informative metabolic profiles (50).

Thesis Plan

The studies were performed with cultures of HepG2 cells – a model for HCC. To inhibit NADPH production via the PPP in these cells, we used polydatin, a known inhibitor of glucose-6-phosphate dehydrogenase. To verify this inhibition, we quantified glucose-6-phosphate dehydrogenase activity. In order to understand the effects of inhibiting oxidative PPP activity on intermediary metabolism and redox state, we used [U-^{13}C]glucose to quantify carbon transfer to lactate and alanine via glycolysis, as well as its utilization as an oxidative substrate by the Krebs cycle. To assess the impact of blocking NADPH production via the PPP on intracellular redox status, we evaluated the protein levels of key proteins related to redox state and quantified selected metabolites whose levels were strongly influenced by intracellular redox state.

With these approaches, we tested the hypothesis that inhibiting NADPH generation via the PPP perturbs both glucose metabolism and intracellular redox state, thereby inhibiting cancer growth.

Experimentally, effects of glucose-6-phosphate dehydrogenase inhibition by Polydatin in HepG2 cells were assessed by measuring the following parameters:

a) Cell growth rates
b) Glycolytic rates and glucose consumption.
c) Glucose utilization by the Krebs cycle evaluated by glutamate ^{13}C-isotopomers.
d) Changes in intracellular metabolite profile related to alterations in cellular redox state.
e) Changes in metabolite concentrations in the extracellular media.

Materials & Methods

Materials and Reagents

All chemicals were of analytical grade and were obtained from Merck, unless stated otherwise. Plastic tissue cultured dishes were from Avantor. Fetal bovine serum, penicillin/streptomycin solution and glutamine were obtained from Sigma. D5030 media was obtained from Sigma and mixed with glucose, glutamine, sodium bicarbonate, Hepes. Deuterated water, [U-^{13}C]glucose and [U-^{2}H]glucose was obtained from Cambridge Isotopes via Tracer Tecnologías Analíticas, S.L.

Cell Cultures

Starter HepG2 cells were washed with sterile PBS and were detached with 0.05% Trypsin for 5 minutes for 37°C. After this incubation, the cells were centrifuged for 5 minutes at 12000 g. The cells were then resuspended in media and an aliquot (10 µL) was mixed with trypan blue for cell count on the TC20 automated cell counter (Bio-Rad, USA). For NMR protocol optimization, HepG2 cells were incubated in 100 mm plates with a density of 45k/cm^3 for 24h for seeding in a DMEM media with the following concentrations: Glucose- 5 mM; L-glutamine- 6 mM; Sodium Bicarbonate- 44 mM; Hepes- 5mM; 10 % (v/v) FBS; 1 % (v/v) Penicillin-Streptomycin. After this seeding, the cells were incubated for 48h with the same media except that the glucose concentration was 10 mM.

For obtaining growth curves, HepG2 cells were incubated in a 96 well microplate following the experiment procedure described for cell culture for NMR protocol optimization. For these ands all subsequent analyses, the cell cultures were kept at 37 °C in an atmosphere of 95 % O_2/5 % CO_2.

For toxicology assays, HepG2 cells were seeded for 24 h in a 96-well plate with the culture medium described for protocol optimization containing 10 mM glucose. The medium was then replaced with an array of media containing 8 different polydatin concentrations (1 mM; 0.5 mM; 0.25 mM; 0.125 mM; 0.0625 mM; 0.03125 mM; 0.015625 mM; 0 mM) distributed among the wells so that for each concentration there were 12 wells. The cells were quenched at 51 hours of incubation.

For the glucose-6-phosphate dehydrogenase activity assay and Western Blot, HepG2 cells were cultured for 48 hours in 60 mm plates in DMEM media identical to that used in the toxicology assay but with two concentrations of Polydatin (0.35 mM and 0.1mM).

For NMR analysis, the cells were incubated in DMEM, following the same experimental procedure described to the G6PD activity assay with the glucose enriched to 50% each with [U-^{13}C]glucose and [U-^{2}H]glucose and with 0.35 mM and 0.1 mM of Polydatin.

Cell harvest and extraction

For NMR analysis, the media was aliquoted for NMR analysis and the rest was discarded and the cell mass was washed with ice-cold phosphate-Buffer solution (PBS), followed by quenching with an ice-cold methanol/water solution (2:1) and transferred into a 2 mL Eppendorf tube by gently scraping the plate. The suspension was then centrifuged for 5 minutes at 4 °C and 12000 g and the supernatant, containing the hydrophilic metabolites, was removed, and reserved. The pellet, containing the cell protein, was stored at -80 °C. The aqueous and organic fractions were dried and stored in -20 °C.

Sulforhodamine B (SRB) assay

After incubation, the culture media was removed and the cells were washed with a PBS solution at room temperature, followed by an overnight incubation with 1% acetic acid in methanol at -20 °C. The plate was then washed and dried at 37 °C. A 0.005 % (w/v) SRB solution was added to each well and incubated at room temperature for 1 hour. The plates were then rinsed with 1 % (v/v) acetic acid to remove unbound dye and dried at 37 °C. To solubilize the protein-bound dye, a 10 mM Tris base solution (pH 10) was added (100 µL to each well) incubate for 30 minutes, followed by a measurement of optic density (OD) at 510 nm in a Cytation 3 microplate reader (BioTek Instruments Inc. USA).

Resazurin assay

Cell culture media was removed, and the plates washed with PBS solution. A solution of Resazurin, 10 µg/mL, was added to each well and the plate was incubated for 1h in a dark room at 37 °C. The fluorescent signal was read using 540 nm excitation and 590 nm emission in a Cytation 3 microplate reader (BioTek Instruments Inc. USA).

Protein quantification

To the weighed pellet, 30 % KOH 1µL/ mg pellet was added, and the mixture was incubated for 1 hour at 70 °C. A 25 µL aliquot was taken for protein quantification using the Bio-Rad BCA kit, according to manufacturer guidelines. Briefly, each sample (in 10 times dilution) and calibration standard (8 µL, in duplicates) were loaded into a 96-wells microplate, followed by an addition of 200 µL of BCA solution (50-parts solution A and 1-part solution B). The

absorbance was read at 562 nm emission in a Cytation 3 microplate reader (BioTek Instruments Inc. USA) and the amount of protein was determined against a BSA calibration curve.

G6PD activity assay

This method is an adaptation of a standardized method from the World Health Organization, coupled with a resazurin probe, due to fluorescence from other cellular components that coincide with that of NADPH. By coupling with a resazurin probe, the NADPH readout wavelength was shifted to a spectral region with less interference, providing a more accurate measurement (51–53).

After the protein quantification, the pellet obtain was diluted was diluted in a Working Buffer to have an amount of 20 µg of protein for each sample, consisting of 50 mM Tris and 1 mM $MgCl_2$ at pH = 8.1, and added, in duplicate, to black microplate. The microplate was read at 570 nm wavelength of excitation against 600 nm wavelength of emission. After this reading 100 µL of Assay buffer, consisting of 3.2 mM $NADP^+$, 6 mM Glucose-6-phosphate and 1 mg/mL Resazurin in Working Buffer, followed by a reading with the same wavelength for 20 min with reading every 30 s.

Western Blot

The pellets obtain from the cell extraction were resuspended in RIPA buffer (50mM Tris pH 8.0, 150 mM NaCl, 5mM EDTA, 15mM $MgCl_2$ and 1% TritonX-100) supplemented with 0.5 mM phenylmethylsulphonyl fluoride (PMSF), 20 mM sodium fluoride (NaF), 10 mM nicotinamide (NAM), 5 mM sodium butyrate, 0,5 % sodium deoxycholate (DOC) and Protease Inhibitor Cocktail (PIC, 2 µL/mL) and an aliquot was taken for protein quantification. After denaturation at 95 °C for 5 min in Laemmli buffer (161-0737, Bio-Rad), an equivalent amount of proteins (20 µg) was separated by electrophoreses SDS–polyacrylamide gels (SDS–PAGE) and transfer in to polyvinylidene difluoride (PVDF) membrane. The membranes were then blocked for 2 hours at room temperature in 5 % BSA in TBS-T (50 mM Tris–HCl, pH 8; 154 mM NaCl and 0.1 % tween-20) and marked with Ponceau Red, to see the protein content of each sample. After that, the membranes were washed in TBS-T and incubated overnight at 4 °C with the antibodies directed against the denatured form OXPHOS complexes cocktail (1:1000, ab110411, Abcam), HKII (1:1000, mAb #2867, Cell Signalling) TOM-20 (1:1000, sc-17764, Santa Cruz Biotechnology), α-Tubulin (1:1000, T6199, Sigma), G6PD (1:1000, sc-373886, Santa Cruz)Biotechnology), Actin_1 (1:1000, MAB1501, Millipore), IDH2 (1:1000, Santa Cruz Biotechnology). Once incubation was completed, membranes were washed with TBS-T

and incubated at room temperature with anti-rabbit (1:5000, 1677074S, Cell Signalling) or anti-mouse (1:5000, 1677076S, Cell Signalling) HRP-conjugated secondary antibodies. Clarity Western ECL Substrate (1705061, Bio-Rad Laboratories) was used for chemiluminescence detection. The densities of each band were calculated with ImageJ Software (version 1.53r 21 – April 2022) and normalized against the densities from the Ponceau Red staining.

NMR analysis

The dried samples were dissolved in 485 µL of $^{2}H_2O$ and 125 µL of 10 mM sodium fumarate internal concentration and chemical shift standard and loaded into 5 mm NMR tubes.

^{1}H and ^{13}C NMR analyses were performed in 11.7 T Bruker NMR Advance III HD system using a 5 mm BB-probe. ^{1}H spectra at 500.1 MHz were acquired with a 45-degree pulse, 10 kHz spectral width, 3 seconds acquisition time and 10 seconds pulse delay. 32 free-induction decays were collected for each spectrum. The spectra were processed with 0.2 Hz line-broadening before Fourier transformation. ^{13}C NMR spectra at 125.8 MHz were acquired with a 90-degree pulse, ~3 kHz spectral width, 4 seconds acquisition time and 5 seconds pulse delay. 10,752 free-induction decays (fid) were collected for each spectrum. The spectra were processed with 1 Hz line-broadening before Fourier transformation.

Processing and integration of ^{1}H NMR spectra was performed with Bruker TopSpin 4.1.4, whereas the processing and integration of ^{13}C NMR spectra was performed in NUTS pro. For the ^{1}H metabolomics analysis, the spectra were pre-processed in ACDLABS 12, with an intelligent binning of 0.01-0.04 ppm intervals before multivariate analysis.

Metabolic analysis

For the media samples, glucose consumption and lactate production were assessed by quantification of resolvable glucose and lactate ^{1}H signals throughout the experimental time compared against a fumarate internal standard (IS), at 6.5 ppm. ^{1}H signals from [U-^{13}C]α-glucose (36% of total glucose) appear as ^{13}C-^{1}H-coupled doublets, at 5.35-5.40 ppm, while the ^{1}H signals from [U-^{13}C]lactate also appear as appear as ^{13}C-^{1}H-coupled multiplets at 1.16-1.20 ppm. After adjusting for hydrogen stoichiometry between IS and metabolite and the fractional enrichment of the [U-^{13}C]glucose precursor, media glucose levels were calculated as follows:

$$[U\text{-}^{13}C]\text{Glucose (mmol)} = \text{IS(mmol)} \times (^{13}C\text{-H1}\alpha \text{ signal/fumarate signal}) \times 2 \times 1/0.36 \times T/A \quad (5)$$

Where IS(mmol) was the amount of fumarate IS in the sample; 2 accounts for the hydrogen

stoichiometry of fumarate relative to glucose H1, 1/0.36 accounts for the fraction of the α-glucose anomer and T/A was the total media volume divided by the volume of the aliquot taken for NMR measurement.

The amount of medium [U-^{13}C]lactate was calculated as follows:

[U-^{13}C]Lactate (mmol) = IS(mmol) × ($^{13}CH_3$ lactate signal/fumarate signal) × 3 × T/A (6)

Where 3 accounts for the hydrogen stoichiometry of fumarate relative to lactate CH_3

From the amounts of glucose and lactate measured over time, the rates of glucose disappearance and lactate appearance were calculated and adjusted to the amount of cell protein per culture plate. Since glycolytic metabolism of glucose generates two equivalents of pyruvate, with the majority converted to lactate, the fraction of disappeared glucose that underwent glycolysis was estimated as the difference between glucose disappearance and 2 × lactate appearance:

Glycolytic fraction (%) = 100 × (Glucose disappearance rate / 2 × lactate appearance rate) (7)

The fraction of disappeared glucose that was utilized by other pathways (including glycogen synthesis, oxidation by the Krebs cycle and nucleotide biosynthesis) was estimated as the difference:

Utilization by other metabolic pathways (%) = 100 - Glycolytic fraction (8)

^{1}H NMR signal assignments and metabolite identification were performed using the Human Metabolome Database and Chenomx NMR suite 9.0 chemical compounds' libraries. For the aqueous cellular extracts, total alanine enrichment, lactate-to alanine ratio, phosphocreatine-to-creatine ratio were determined from analysis of their ^{1}H NMR signals. Acetyl-CoA enrichment was assessed by ^{13}C NMR analysis of glutamate present in the aqueous cellular extracts, and it was given by Equation 9,

$$Acetyl - CoA\ enrichment = C_4Q * \frac{C_4F}{C_3F} \quad (9)$$

where C_4Q represents the glutamate carbon 4 quartet signal representing glutamate isotopomers with ^{13}C in carbons 3, 4 and 5 C_3 and C_5; C4F was the total signal area of the glutamate carbon 4 multiplet and C_3F was the total area of the glutamate carbon 3 multiplet (54).

Statistical analysis

All data were analysed via Prism 8.0.2. The multivariate analysis was performed with MetaboAnalyst 5.0 online software (https://www.metaboanalyst.ca) for PCA and PLS. For the PLS analysis, Q^2, R^2, and the p-value of the permutation testing (1000 permutations) were used as quality parameters for the regression model. Models that achieve both a $Q^2 > 0.3$ and $p < 0.05$ were considered as valid following the recommendation by *Triba et al. (2015)*. On valid models, the variable important in projection (VIP) with the score value higher than 1 were assigned as contributing to the observed group clustering. All scores plots (PCA and PLS models) were drawn at the 95% confidence level.

Results

Protocol Optimizations

Before studying the effect of polydatin-mediated PPP inhibition on cellular metabolism, we first established the optimal experimental conditions in terms of starting glucose and polydatin concentrations for these studies. One important constraint was the high cost of [U-^{13}C]and [U-^{2}H]glucose tracers that placed an upper limit of 10 mM to the glucose concentrations that could be used in our studies. Within this limit, the main consideration was to maximize linear cell growth rates over the 24 hr incubation period without the culture reaching confluence. Under these conditions, the isotopically enriched glucose was metabolized in sufficient amounts to significantly enrich the intracellular metabolite pools under conditions where the cells have maximum metabolic activity. This provides the best opportunity for NMR observation and quantification of metabolite isotopomers and analyses glucose fluxes. Figure 7 shows a comparison of 5 *vs* 10 mM starting glucose levels on cell growth rates. With 10 mM glucose, the cell mass of HepG2 increased around 2.6 times compared with 5 mM with growth being linear out to 72 hours.

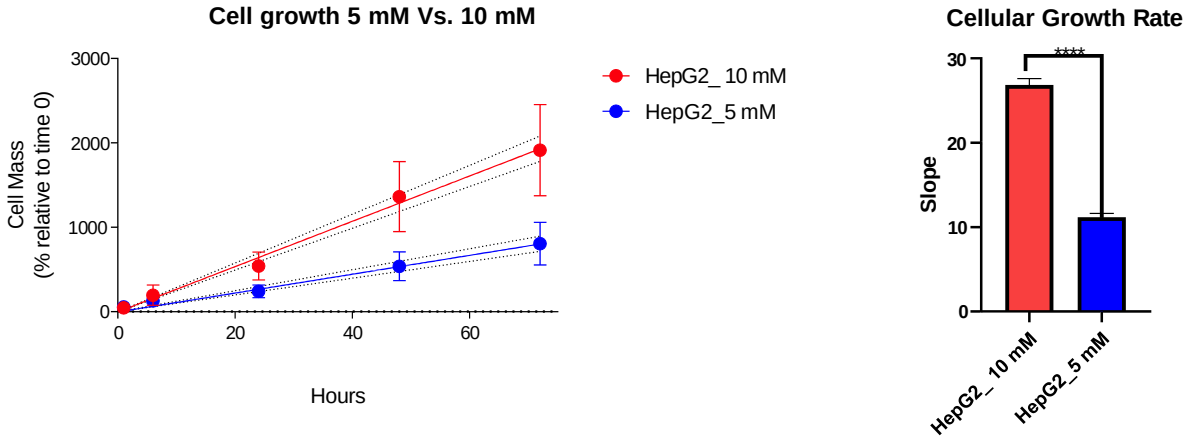

Figure 7 Baseline corrected cell growth 10 mM vs 5 mM over time. In this graphic was possible to see that HepG2 cell have much higher cell mass in glucose concentration of 10 mM relative to 5 mM. Welch t test, **** p-value = 0.0001 N=4

On this basis, we selected a starting glucose concentration of 10 mM, which represented the best compromise between sustaining optimal cell growth and the cost of each experiment in terms of the isotopically labelled glucose tracers.

The next step was to optimize the Polydatin concentration. We incubated HepG2 cells for 48 hours with different Polydatin concentrations and cells were analysed with SRB assay to assess cell mass and metabolic activity (Figure 8). The polydatin dose that diminished metabolic activity by half was 0.3591 mM and the dose that halved cell mass growth was 0.3060 mM. Based on these results, we chose two concentrations to test the effect G6PD activity: one being the LD_{50} concentration of 0.35 mM and the other being 0.1 mM - the highest concentration that did not significantly impact cell metabolic activity and mass.

We then determined the effect of these two selected polydatin concentrations on cellular growth and G6PD activity (Fig. 9).

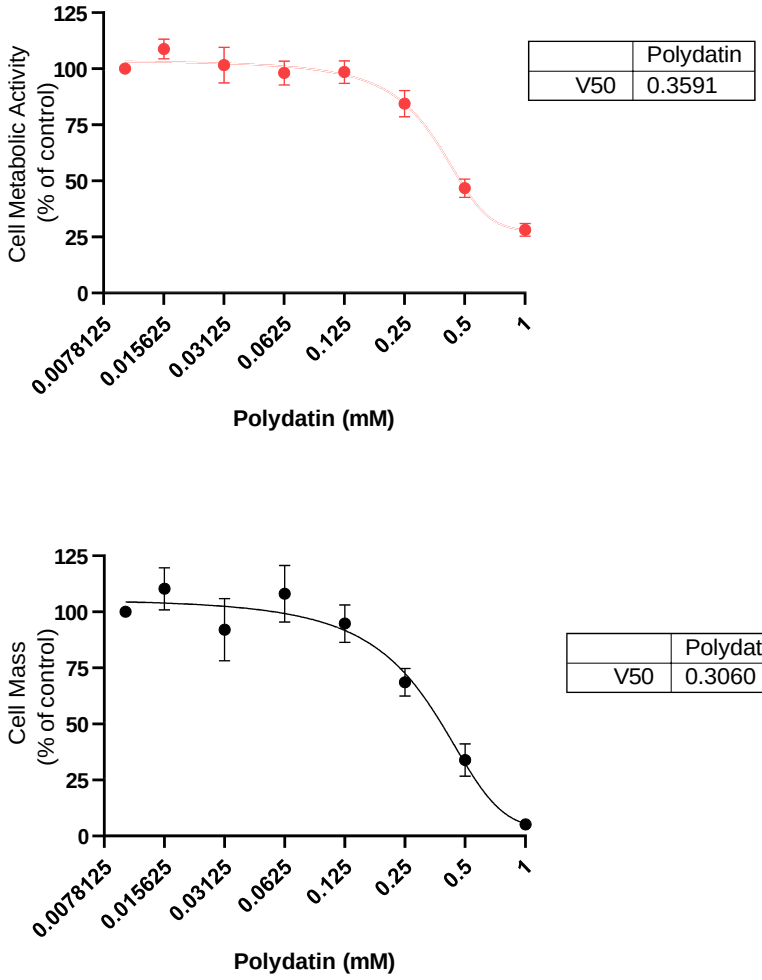

Figure 8 Effects of different polydatin concentration on cellular metabolic activity (as measured by Resazurin assay) and cell mass as measured by.) with the calculated doses for 50% decrease (V50) also shown. 8 determinations were made per concentration and data were shown as means with error bars representing standard deviation.

There were no significant differences in G6PD kinetics between control cells and cells incubated with either polydatin concentration although there was a tendency for a lower rate for 0.35 mM compared to 0.1 mM polydatin. There was a significant reduction in cell mass growth of cells incubated with 0.35 mM polydatin compared to those incubated with 0.1 mM polydatin as well as controls. We also determined 48 hours as the best incubation time for the experiment, since cell mass growth was linear during this period with or without 0.1 mM polydatin. Based on these results, we explored the effects of these two polydatin concentrations on cellular intermediary metabolism in subsequent studies.

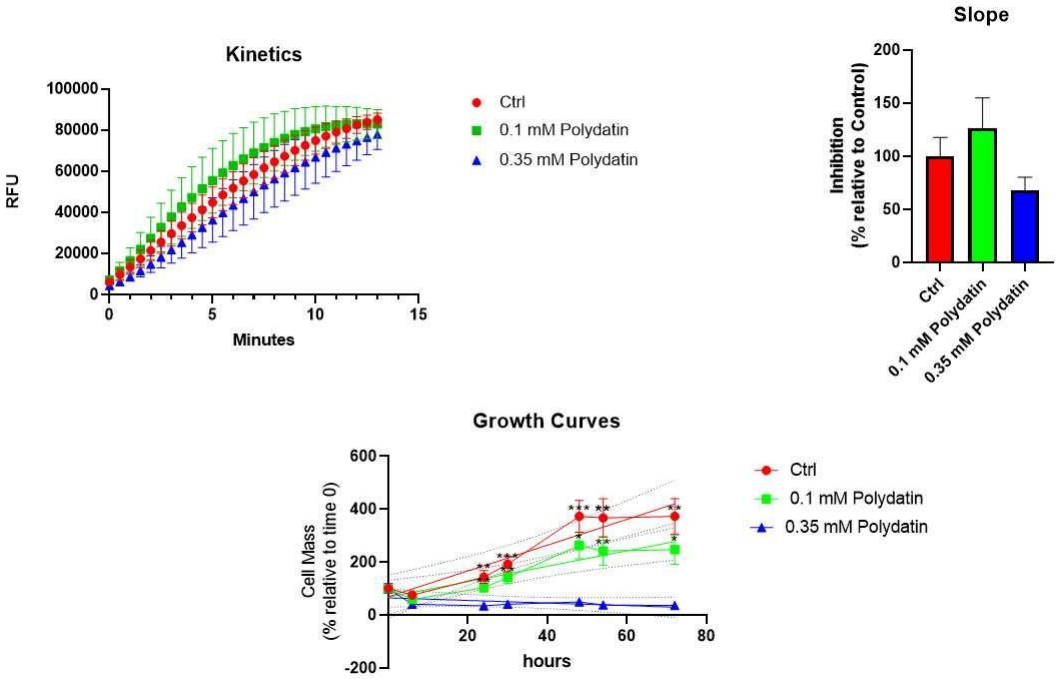

Figure 9 Analysis of Polydatin effects on HepG2 cells (0,1 and 0.35 mM), both in terms of G6PD kinetics (n=4 per condition) and in cellular growth rates (n=8 per condition). For the growth curve, Mean ± SEM, for 24,32 48 and 72 hours Brown-Forsythe and ANOVA,* p-value ≤ 0.05, ** p-value ≤ 0.01,*** p-value ≤ 0.001 N=4 For 48 hours, Kruskal-Wallis * p-value ≤ 0.05, *** p-value ≤ 0.001, N=4-8

Effect of polydatin on glucose metabolism

In order to better understand the effect of Polydatin on glucose metabolism, the cells were incubated with 10 mM of glucose (5 mM of [U-^{13}C]glucose and 5 mM of [U-^{2}H]glucose) with 0.1 mM and 0.35 mM of polydatin for 48 hours. Samples were collected from extracellular media, throughout the incubation, and intracellular media. The samples from the extracellular were analysed by ^{1}H NMR and metabolomics, whereas the intracellular media (extracts) were analysed ^{1}H NMR and ^{13}C NMR.

For the media, the ^{1}H NMR spectra was represented in Figure 10. From these signals, we obtained estimates of glucose consumption, lactate production, glycolytic and non-glycolytic rates, represented in figure 11.

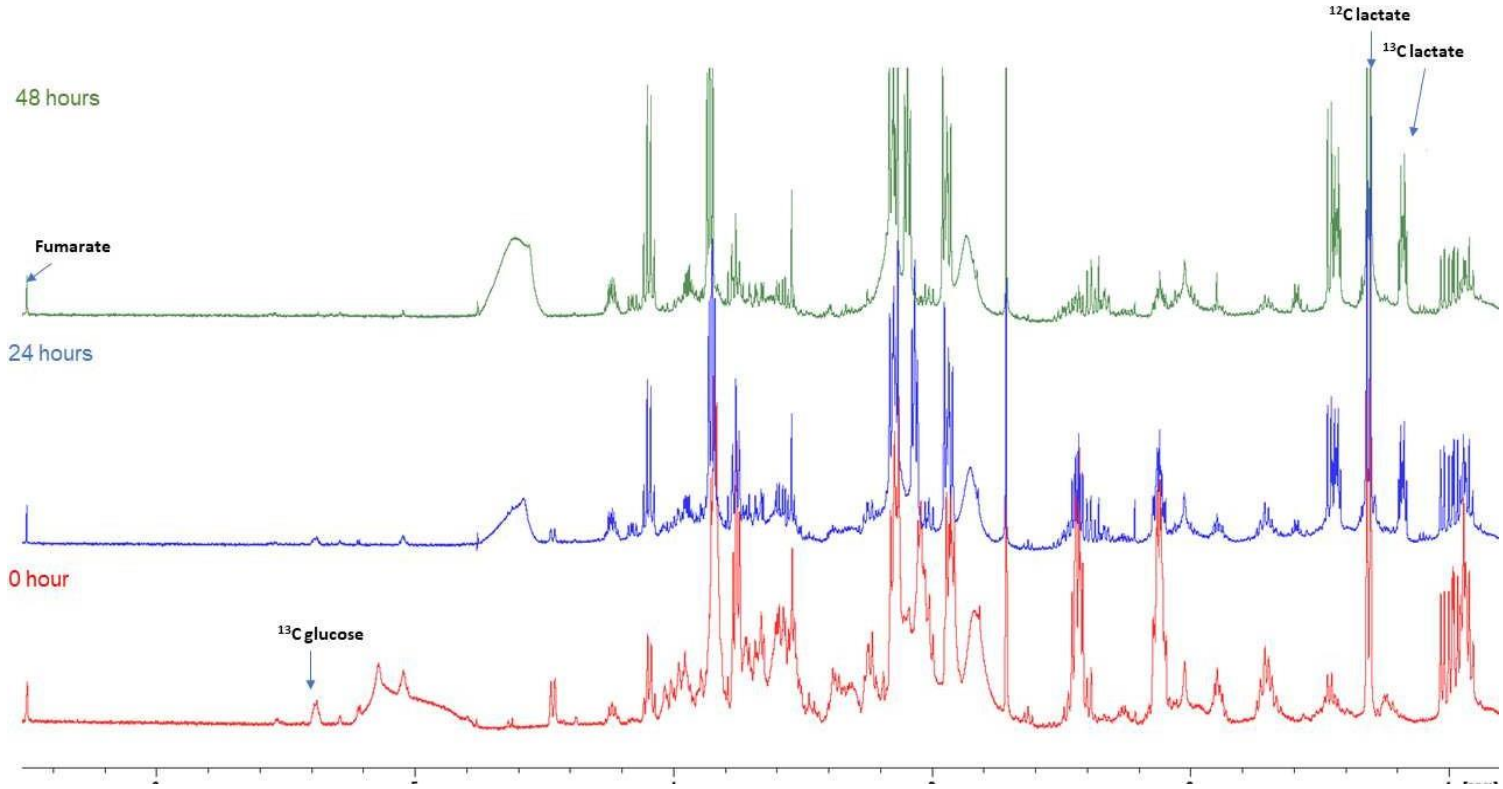

Figure 10 ^{1}H NMR spectra of media control sample in 3 different time point (0, 24, 48 hours). Although not represented in this figure the samples collected at time 8 and 32 hours were also included in the analysis.

In terms of glucose consumption and lactate production, the cells with 0.35 mM Polydatin there were no significant changes in both glucose consumption and lactate production, although there was a tendency for an increase in lactate production for cells treated with 0.35 mM polydatin compared to 0.1 mM polydatin (*p*-value = 0.077). Cells treated with 0.35 mM polydatin also exhibit a higher percentage of glucose being diverted to lactate compared with cells treated 0.1 mM of polydatin and a correspondingly lower percentage of glucose being consumed by other pathways. The cells treated with 0.35 mM of polydatin also exhibit a tendency for the same metabolic phenotype when compared to control cells (*p*-value = 0.0604).

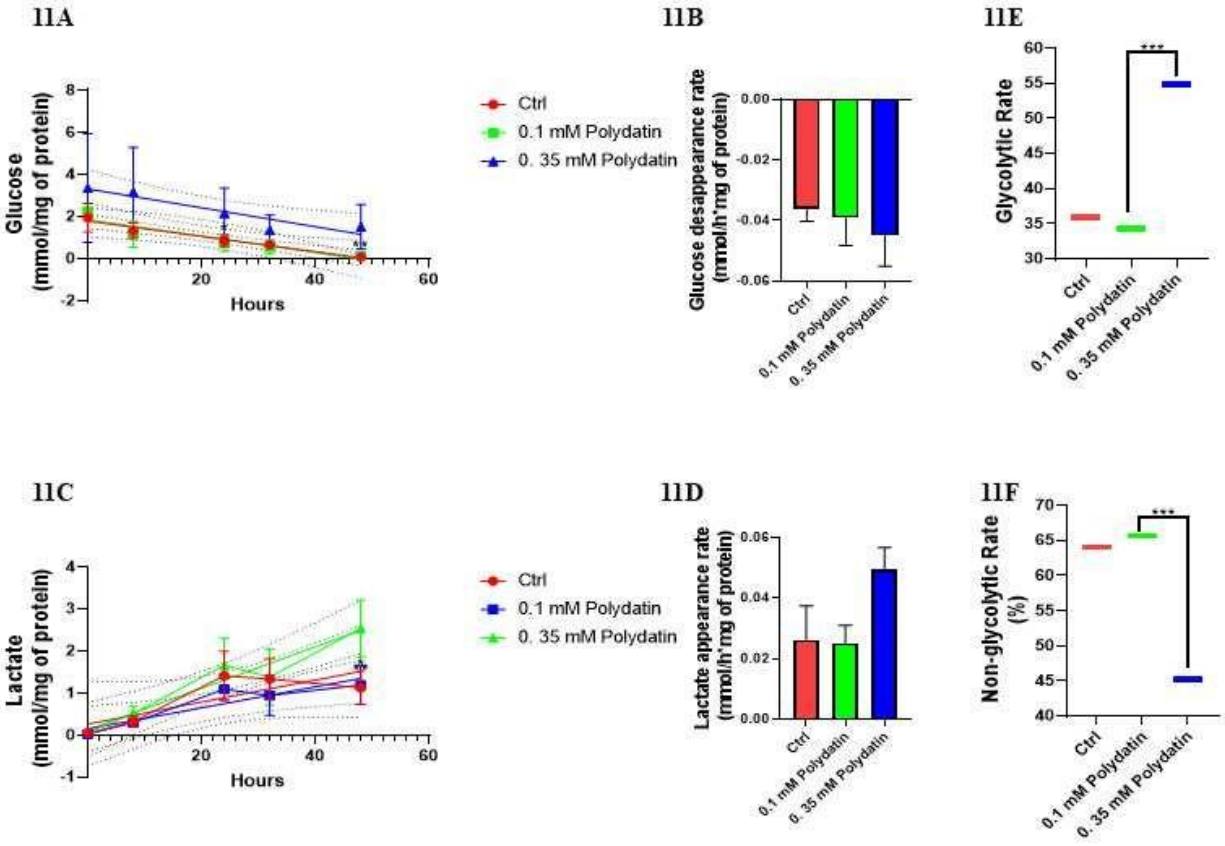

Figure 11 *Effects of Polydatin on glucose consumption and lactate production. 11A: Glucose levels measured over 48 hours; 11B Glucose disappearance rates measured over 48 hours; 11C Lactate appearance measured over 48 hours; 11D Lactate appearance rates measured over 48 hours. 11E Fraction of glucose metabolized to lactate (%); 11F fraction of glucose metabolized to other products (oxidative phosphorylation and/or biosynthetic pathways). In figures 11A and 11C, they grey dot represent the confidence limits for the linear regression*

In order to discover additional metabolic features of the media samples that might be contained in the ^{1}H NMR signals, we performed unsupervised and supervised metabolomic analyses of the ^{1}H signals. In figure 12, there were represented the PLS-DA for 0.1 mM Polydatin vs. 0.35 mM Polydatin, Control vs. 0.1 mM Polydatin, Control vs. 0.1 mM Polydatin vs. 0.35 mM Polydatin. From the VIP scores from each PLS-DA, we were able to identify the best 3 metabolites, which were represented in table 1. All quality parameters for the validation of the PLS-DA and PCA were showed in the **Appendix.** There was an unexpected separation in time 0, which may be due to the presence of polydatin and its vehicle, DMSO.

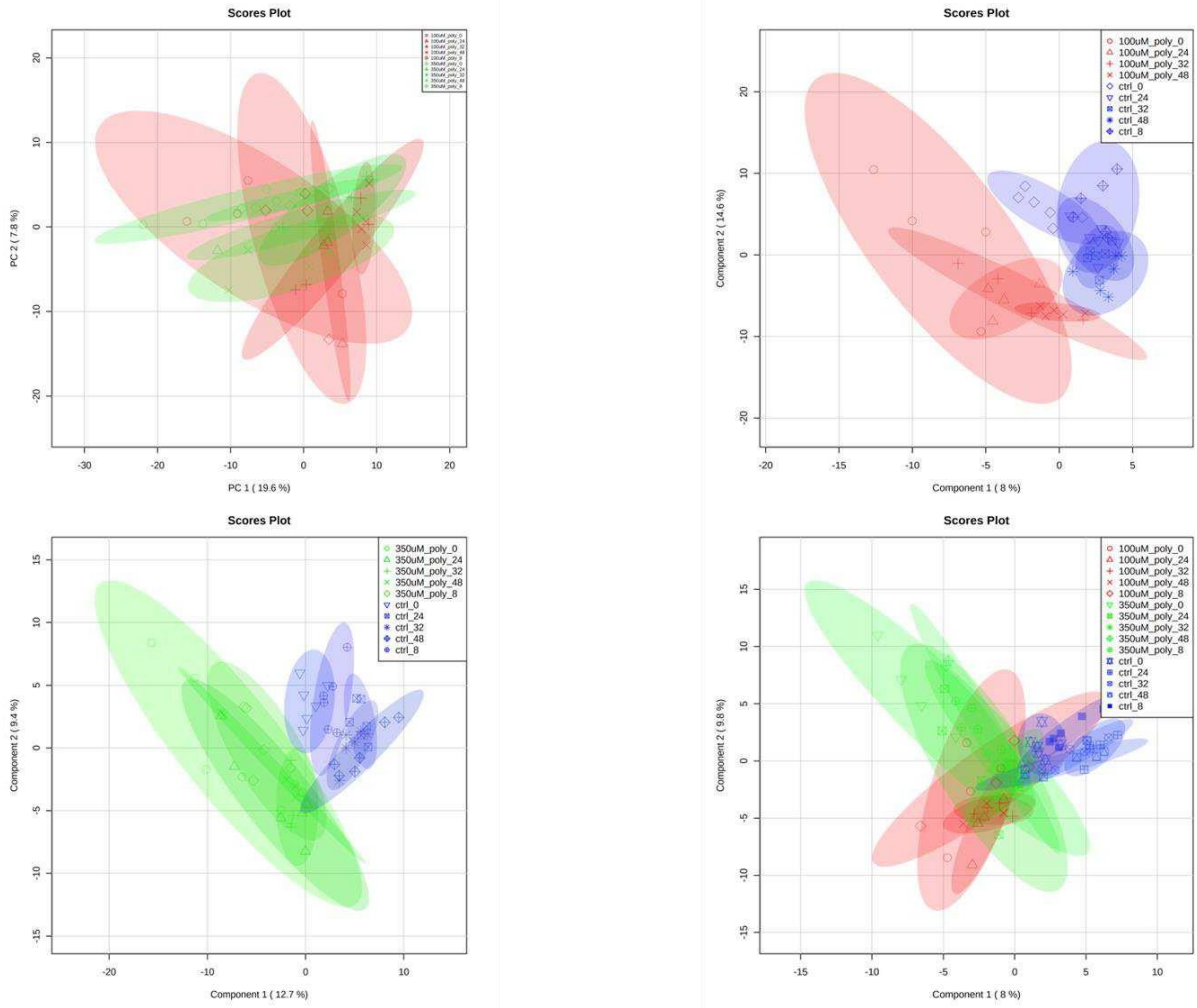

Figure 12 PLS-DA for 0.1 mM Polydatin vs. 0.35 mM Polydatin, Control vs. 0.1 mM Polydatin, Control vs. 0.1 mM Polydatin vs. 0.35 mM Polydatin.

We quantified and analyzed the 3 metabolites and their results were represented in figure 13. In terms of ^{13}C Lactate there was a significant increase in 0.35 mM polydatin against Control (0.35 mM Polydatin: 4.232 ± 0.4620 vs. Control: 1.875 ± 0.2702 p- value= 0.0067; N= 4-6) and 0.1 mM Polydatin (0.35 mM Polydatin: 4.232 ± 0.4620 vs.0.1 mM Polydatin: 1.590 ± 0.4958 p-value= 0.0077; N= 4-6). The same occur in the case of tyrosine, where there was an increase between 0.35 mM μand control (0.35 mM Polydatin: 0.3617 ± 0.05300 vs. Control: 0.1250 ± 0.01945 p-value= 0.0153; N= 4-6) and 0.1 mM and Polydatin (0.35 mM Polydatin: 0.3617 ± 0.05300 vs. 0.1 mM Polydatin: 0.1250 ± 0.01945 p-value= 0.0153; N= 4-6). As ^{13}C alanine, there was a significant increase between 0.35 mM Polydatin and 0.1 mM Polydatin (0.35 mM Polydatin: 0.9100 ± 0.1148 vs. 0.1 mM Polydatin: 0.3840 ± 0.1269 p-value= 0.0413; N= 4-6).

Table 1 Best 3 metabolites result from the VIP scores

Peak	Chemical shift	Identification
1	1.59	[U-^{13}C]alanine
2	7.5	Tyrosine
3	1.1	[U-^{13}C]Lactate

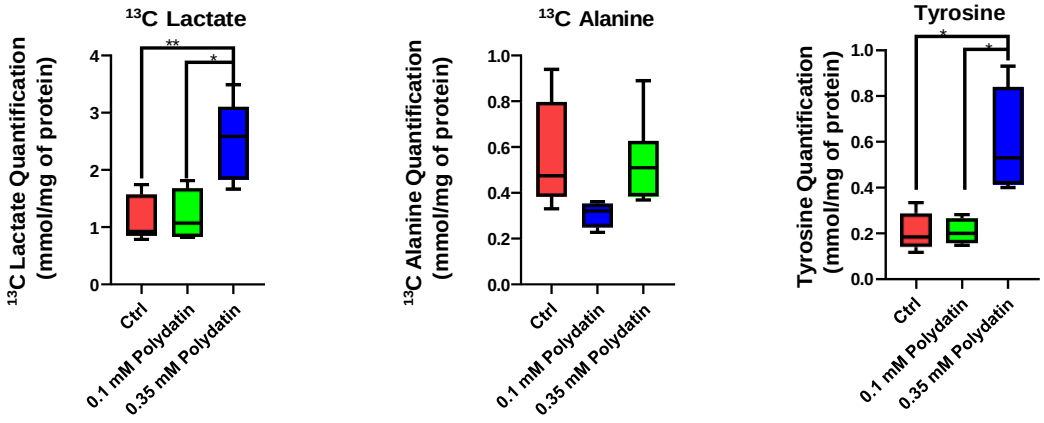

Figure 13 Quantification of the 3 metabolites from PLS-DA. Brown-Forsythe ANOVA test, * p-value < 0.05, ** p-value < 0.01

We also analysed the extracts by ^{1}H and ^{13}C NMR isotopomer analysis. The ^{1}H and ^{13}C NMR spectra were represented in figure 14. There were some changes in the aqueous extracts when compared to media sample in ^{1}H NMR. One of which was the presence of alanine both unlabelled and ^{13}C labelled in the extracts, while in the media the presence was minimal.

Another example was tyrosine which as mentioned before was increased in media sample, but there were no significant changes in extracts between the different groups (data not showed). There was also a very low glucose signal, both in ^{1}H and ^{13}C spectra, which reflects total glucose consumption when it was uptaken by the cells.

In the ^{13}C spectra there are represented the main metabolites. These labelled metabolites are also visible in the ^{1}H spectra as you see in the figure. For the alanine signal, since it appears in a spectral region with very little peak overlapping it is possible to quantify the satellites, which have a consistent ^{13}C-^{13}C-couppling as the ^{13}C spectra. However, in order to calculated acetyl-CoA enrichment, according to Equation 9. There is a need to analyse carbon signals from C_4 glutamate and this is impossible to do in ^{1}H NMR first because glutamate appear in spectral region with many overlapping metabolites, which renders the quantification unprecise and, due to the bigger spectral window and the fact ^{13}C NMR only detects ^{13}C nucleus, the multiplet resolution of C_4, when signal is sufficient is perfect to perform this type of calculation. There were differences in signal intensity when compared control and cells treated with 0.1 mM of polydatin against cells treated with 0.35 mM of polydatin. In fact, due to lower amount of biological material it was very difficult to achieve a good signal to noise ratio that allowed to make accurate quantification.

.

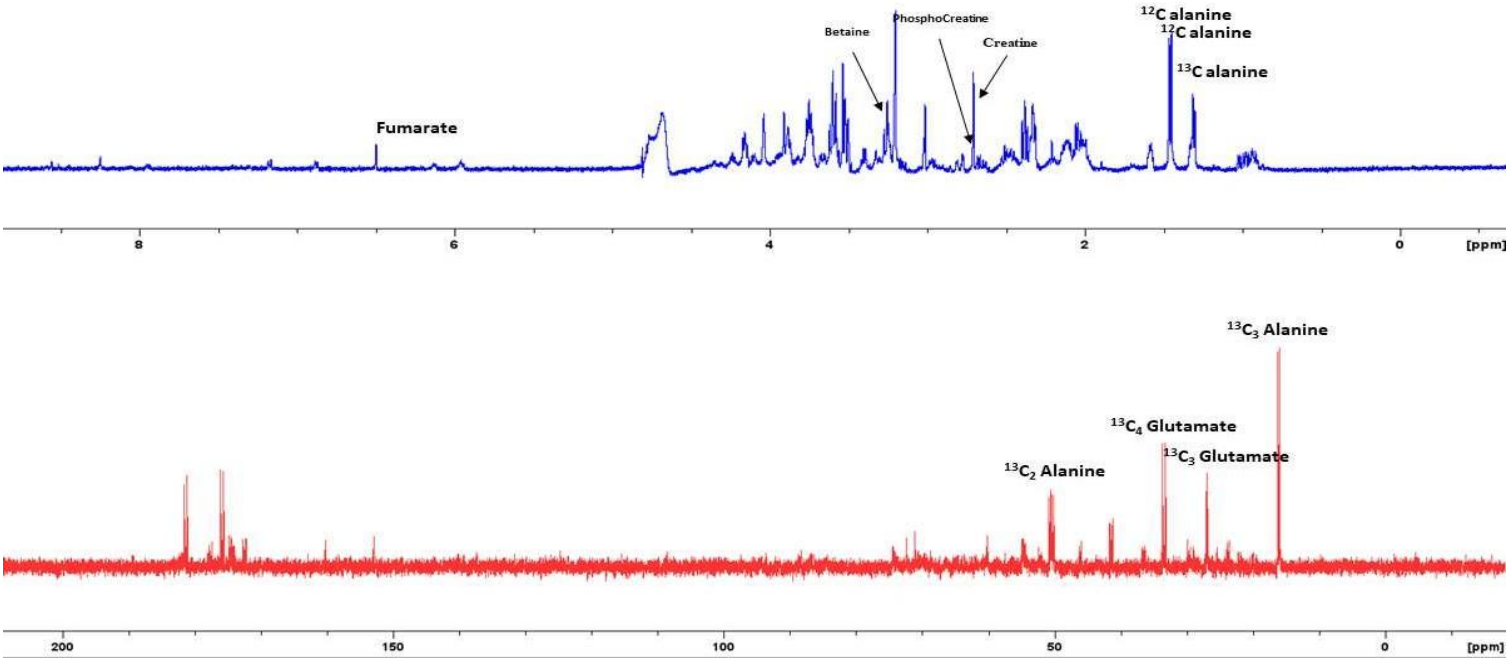

Figure 14 Representative ^{1}H and ^{13}C NMR spectra from an extract of a control cell culture acquired at 11.7 T (500 MHz 1H). The collection time was 6 min for 1H spectrum and 12 hours for 13C NMR spectrum.

^{1}H quantified alanine enrichment, Phosphocreatine to creatine ratio and Betaine quantification (Fig.15). There were no significant changes in alanine enrichment. As for phosphocreatine to creatine ratio there was a slight increase in cells with 0.35 mM of polydatin when compared to cells with 0.1 mM of polydatin

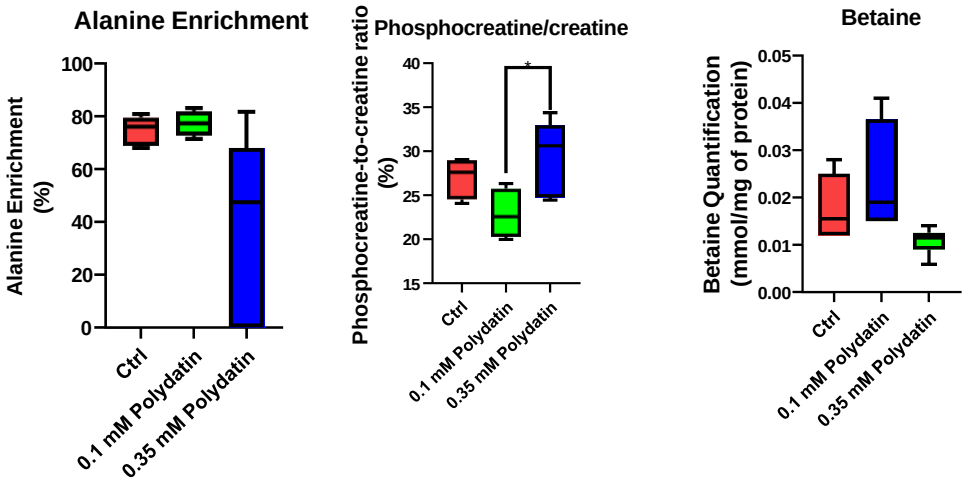

Figure 15 Effects of Polydatin on intracellular media. It was possible to see a increase in Phosphocreatine to creatine and a decrease in Betaine quantification in cells with 0.35 mM of Polydatin when compared to cells with 0.1 mM Polydatin. Phosphocreatine/creatine: Brown-Forsythe ANOVA test, * p-value < 0.05, N= 4-6..

From the glutamate signals in the ^{13}C NMR spectra we assessed the contribution of [U-^{13}C]glucose to acetyl-CoA under the different conditions and the results were shown in (Fig.16). These results were normalized to the total amount of glucose, given the [U-^{13}C]glucose only accounts for half of the total glucose amount given to the cells.

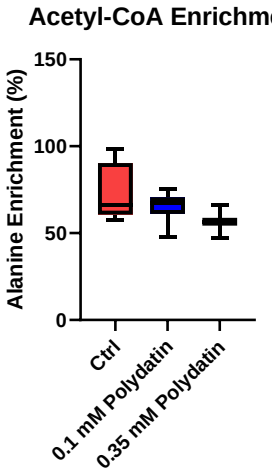

Figure 16 Effects of Polydatin on Acetyl-CoA enrichment. Kruskal-Wallis test, N = 2-6

We also determine expression of several proteins associated with metabolic pathways, which were represented in Fig.17. Hexokinase II, which catalysed the first step of glycolysis; Tom-20 which is a protein associated with mitochondrial importation; Isocitrate dehydrogenase 2, which is a mitochondrial NADP-dependent protein that catalysed the conversion of α-ketoglutarate into isocitrate and glucose-6-phosphate dehydrogenase which catalysed the step limiting reaction of PPP and is the enzyme that polydatin, reportedly, inhibit There was no significant difference in Hexokinase II and Tom-20. There was a significant decrease in Isocitrate dehydrogenase II in cells with 0.1 mM Polydatin and with 0.35 mM Polydatin compared to Control. In terms of Glucose-6-phosphate dehydrogenase, there was no significant changes, however we were not able to determine expression levels for G6PD in cells with 0.35 mM Polydatin. All Western blots images were represented in the Appendix.

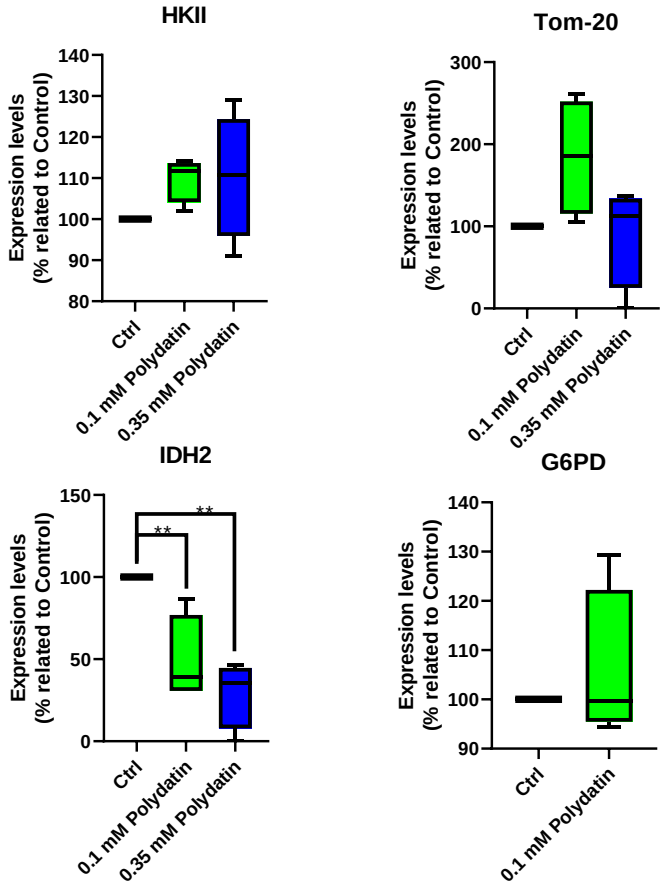

Figure 17 Effect of polydatin on the expression of selected related to intermediary metabolism of glucose and other substrates. HKII, Tom-20, IDH2: Ordinary one-way ANOVA, ** p-value < 0.01 N = 4; G6PD: Unpaired t test with Welch's correction, N = 4

Effect of polydatin on cellular redox homeostasis

Given the important role of the PPP in redox homeostasis, we wanted to understand the effect of polydatin on cellular redox state and cytoskeleton, as assessed by the lactate to alanine ratio, and from the expression levels of proteins associated with antioxidant systems and cytoskeleton. These findings were represented in Fig.18. There was a significant increase in lactate to alanine ratio in cells treated with 0.35 mM of Polydatin when compared to Control cells. In terms of protein expression, there was a reduction of Thioredoxin expression roughly by half in cells with 0.35 mM Polydatin when compared to Control and cells with 0.1 mM Polydatin. Cells treated with 0.35 mM of Polydatin also show higher expression levels of SOD1 when compared cells treated with 0.1 mM of Polydatin. There were no significant differences in catalase expression levels.

We also assessed the expression levels for two enzymes in the cytoskeleton. In terms of α-tubulin expression, there was a significant reduction in expression levels in cells treated with Polydatin versus Control cells. Cells treated with 0.35 mM of Polydatin also had a lower expression level of Actin, relative to Control cells.

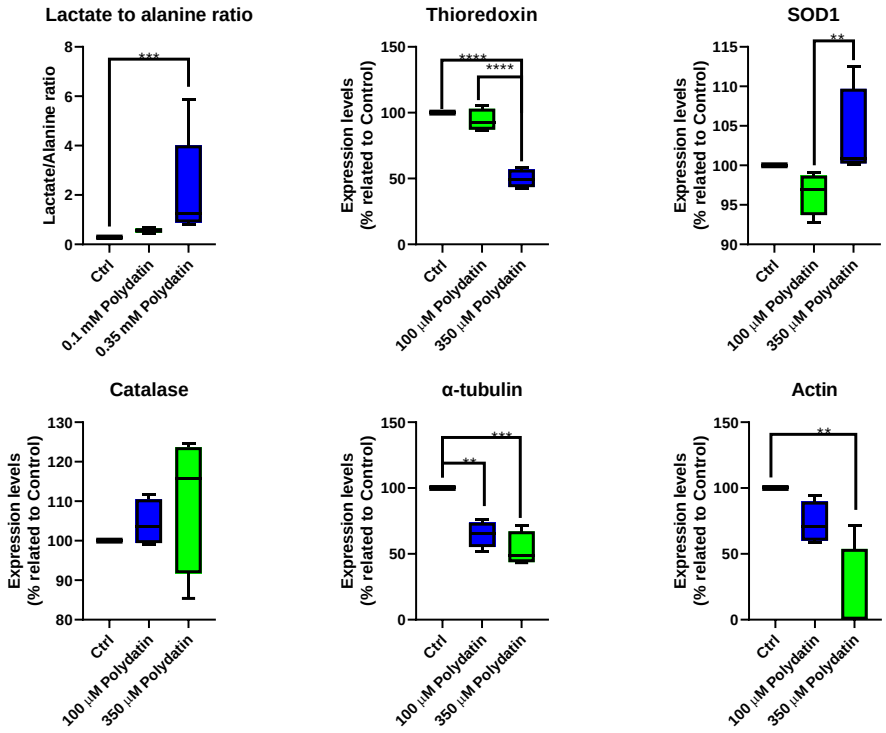

Figure 18 Effects of different polydatin concentrations on lactate to alanine ratio; thioredoxin expression, superoxide dismutase-1 (SOD-1), catalase, α-tubulin and Actin in control cells and cells treated with either 0.1 mM or 0.35 mM polydatin. . Lactate to Alanine ratio and Actin: Kruskal-Wallis test, ** p-value < 0.01, *** p-value < 0.0001, N=4-6 and 4, respectively; Thioredoxin, SOD1, Catalase and α-tubulin: Ordinary One-way ANOVA, ** p-value < 0.01, *** p-value < 0.001, **** p-value < 0.0001, N = 4

Discussion

Protocol Optimizations

The aim of this study was to elucidate the role that PPP may have on cancer metabolism and showcase some of its capabilities as a therapeutical target. We supplemented HepG2 cells, a known cell model for HCC (55), with [U-^{13}C]glucose and [U-^{2}H]glucose for 48 hours. For the sake of this thesis data for ^{2}H NMR isotopomer analysis was not processed. Further analysis would be needed to join the metabolic information gather from ^{2}H NMR spectra. One example of the metabolic information that can be gather from deuterium spectra was the one published by our lab, where we determine that in fatty acids around 50 % of the hydrogens were provided by NADPH (31).

Our PPP inhibitor was Polydatin, a polyphenol derivative from resveratrol, that, according to *Mele et al.* (21) was able to inhibit, *in vitro*, to reduce invasion by 60% and increase apoptosis in 50%. *In vivo* studies, this inhibitor was able to cause a tumour reduction 30% in tongue liver cancer. Moreover, there was a significant reduction in G6PD activity showed by the authors of the study. We perform toxicology assay to determine the best concentration for our studies. The two best concentrations (0.1 mM and 0.35 mM) were used to study the direct effect on G6PD activity. There were no significant changes, probably to the variability in our experimental N. To overcome this setback and clarify on polydatin role on PPP in general, and G6PD in particular, a complementary experiment to the G6PD activity would be needed, as well as the NADPH quantification (or $NADP^{+}$/NADPH ratio) in order to assess the effect direct effect of the PPP inhibition on NADPH homeostasis. *Mele et al.* also showed difference in $NADP^{+}$/NADPH ratio, ally to a decrease in growth and proliferation, as our results showed as well. The growth curves also allow to determine the best incubation time for our experiments. We choose 48 hours since there was no growth in the last 32 hours of incubation.

Effects of Polydatin on glucose metabolism

HepG2 cells were treated with Polydatin to inhibit the step-limiting reaction of PPP. The cells treated with 0.35 mM of Polydatin, showed a tendency for a higher lactate production, which reflects a more glycolytic rate. Given that PPP inhibition reduces biosynthetic pathway, one possibility was that more glucose was being driven to Glycolysis, since was not being used to provide building blocks to biosynthesis. These results were also confirmed by the higher amount of ^{13}C lactate in cells treated with 0.35 mM polydatin compared to both control and 0.1 mM polydatin. One interesting fact was that that none of cells exhibit Warburg-like effect, which was a favour of glycolysis over cellular respiration, even in the presence of oxygen which can

jeopardize their role has a true cancer-like model. One possibility was a hyperoxia (higher oxygen concentration) that favours a more oxidative metabolic profile. This theory was tested by *Van Wensum et al.* where they incubated hepatocytes-like cells (HepaRG) in hyperoxia, 40% O_2, and showed that these conditions increase hepatocyte differentiation, which is characterized by a more oxidative profile, whereas hypoxia favours steam cells-like metabolic profile, which is characterized by a more glycolytic profile. (56)

In order to unravel new metabolites that were sensitive to polydatin, we perform metabolomics analysis on extracellular media. From 4 PLS-DA, we select 15 VIP bins for each PLS-DA. However, we only selected 3 best metabolites for the analysis. These reduction masks possible other metabolic, and other experiments would be needed to have perform a proper identification. *Chen et al.* showed, for example in several cancer cell lines, including HepG2, that knockout of G6PD alter the folate metabolism and that NADPH was required for dihydrofolate reductase activity. Higher concentrations of Polydatin have increased extracellular concentration of labelled lactate and alanine, that, possibly due to slow growth, were not required to sustain biosynthesis and energy needs and were, therefore, exported out of cell. *Bonuccelli et al* propose a model where alternative carbon sources, in this case lactate and ketone bodies, in mammary cancer cells growth and proliferation, in a "Reverse Warburg Effect" (13). 0.35 mM Polydatin cells also showed increase levels of extracellular tyrosine, which can be a lower tyrosine uptake, since it was provided by the DMEM media and there were no significant changes in intracellular tyrosine concentration (data not showed). However, it would be interesting to shed a light on the role of tyrosine in liver since *Ferreira et al.* showed that acute administration tyrosine inhibits malate dehydrogenase, citrate synthase and mitochondrial complexes II, III and IV in both brain and liver.(57)

We also analysed the intracellular media, in order to have a clear sense on how this PPP inhibitor was affecting intracellular metabolism. Based in our results, Polydatin seem to have an in phosphocreatine/creatine ratio. In the first result, phosphocreatine/creatine was known to provide an energy buffering, given that the dephosphorylation of phosphocreatine provides ATP to the cells. Moreover, creatine kinase, the enzyme that catalysed the reaction mentioned above was found to have higher activity in primary HCC patients.(58)

Cancer cells have upregulated anaplerosis sustain growth and proliferation. In this sense, Polydatin does not have an effect on Krebs cycle turnover (data not showed). However, we had a problem with quantifications ^{13}C NMR isotopomer analysis, due to the low S/N that may mask any significant changes in Krebs cycle turnover. Another possible indicator of this hypothesis was the fact that cells treated with Polydatin showed decreased IDH2 expression levels. IDH2 is NADP-dependent mitochondrial enzyme that catalysed the conversion of α-ketoglutarate into isocitrate, and it was found to upregulate in renal cell carcinoma to sustain DNL. Given the close relationship between PPP and DNL, there was a possibility for this pathway to be more

dependent then Glycolysis or Krebs cycle. However, further studies would be needed to test this hypothesis.(28,34).

Effects of Polydatin on Redox homeostasis

PPP, as mentioned before, provides nucleotides for biosynthesis and NADPH for both biosynthetic pathways and redox homeostasis. Cancer cells were known to be prone to ROS accumulation, due to the fast growth and proliferation. Moreover, ROS, in a control dose, have been found to enhance cancer cell survival and proliferation, while high doses promote cancer cell death and stop proliferation. In order to cast a light on this, we study lactate to alanine ratio, a metabolic ratio (used to indirectly assess cellular redox state and $NADH/NAD^+$) and enzymes related to antioxidant response and cellular structural stability. With the increase Polydatin dose was found to shift in lactate to alanine, which reflets a more oxidative environment was consistent with an ROS accumulation, which also can explain the reduction in growth experience by the cells treated 0.35 mM of Polydatin. These cells also experience lower expression levels of thioredoxin when compared to both control and lower Polydatin dose treatment cells. Thioredoxin was reduced by thioredoxin reductase (TRxR), in the presence of ROS, with NADPH as electron donor. TRX overexpression was found to improve immunometabolism in T cells, while the inhibition was found to effective in impairing metabolism and lower growing in leukaemia cells. These results were consistent with ours in the sense lower TRX expression was related to lower growing rates, although not enough to promote a deeper metabolic impairment (59,60). Higher concentration Polydatin also increased superoxide dismutase 1 expression levels. This can be possibly due to a compensatory antioxidant function done by SOD1. In fact, *Fang et al.* showed that low levels of Polydatin can restore SOD1 activity and reduce ROS activity in mice with cholestatic liver injury. This can be adding a new insight into how ROS modelling can have been promising therapeutical approach to cancer cells (61,62).

We also found that PPP inhibition may have on cytoskeleton arrangement via ROS accumulation. Tubulins regulate the activity, for example, oncosuppressor and cellular stress mediator, p53, and can modify microtubule integrity in response oxidative stress to mitigate cell death. This response was consistent with our results that despite the clear lower expression of α-tubulin in lower doses of Polydatin, that may be related to cells ability to maintain cell death to a minimum. Further studies who be needed to determine possible microtubule and cytoskeleton modification in response to ROS accumulation (61,62). High dose Polydatin-treated cells also exhibit lower levels of actin. Actin was found to correlate with HCC aggressiveness and EMT. Given that G6PD overexpression was found to increase invasion by activation of EMT, there was a possible relationship between G6PD and actin expression, heightened the potential of

PPP as a therapeutical target (25,63).

These results sustain the idea that effecting PPP and consequently NADPH promotes a larger effect on redox homeostasis then glucose metabolism. This may support the hypothesis that NADPH production via PPP is a requirement to sustain antioxidant response and glucose metabolism rely on either NADH or NADPH or other sources. Recently *Cheng et al.* showed that in several cancer cells that the loss of G6PD triggers a compensatory upregulation of malic enzyme 1 and isocitrate dehydrogenase 1 for NADPH production. We assessed the expression levels for another NADP-dependent enzyme, ID2, and we showed that, actually, a decrease in expression levels with polydatin. IDH2 is a mitochondrial enzyme, while IDH1 and ME1 are cytosolic enzymes and PPP is a cytosolic pathway as well. This may suggest that this compensatory response may be site-specific. Moreover, since PPP accounts for 45 % of the mitochondrial NADPH, this may be the reason behind the IDH2 lower expression. In order to further test this hypothesis further studies would be needed.(29,30,34,35)

One important aspect of polydatin action was that it resembles a hormetic effect. Hormetic effect was described as phenomenon where a certain agent in low doses acts as stimulator and in higher doses as an inhibitor. Several studies as mentioned the effect of polydatin in lower concentrations to promote antioxidant pathways to protect against advanced glycation-end products or act a cardiac protective agent against burn injury in rats. However, both our results and *Mele et al.* has pointed to higher concentrations of polydatin to promote oxidative stress and consequently cell death. In the first case the *Hang et al.* used 0.005 mM, 0,010 mM, 0,020 mM, which was a much lower concentration when compared to the ones used in our studies (0.1 and 0.35 mM). If we compared the study of *Jiang et al* and the *Mele et al* where the concentration of the latter was times higher for tongue cancer. Moreover, in our results, polydatin showed an inconsistency in PPP inhibition because however not significantly affecting G6PD activity it affects ROS activity, thioredoxin and IDH2 expression, all of which depending on NAPDH bioavailability. Based on this, polydatin does not seem to be the best inhibitor for PPP.(21,64–66)

Conclusion

Our goal in this work was to assess how the NADPH production via PPP would be affected upon inhibition, with polydatin and determine PPP as a potential therapeutical. Based in our results, despite not being the best inhibitor, given the inconsistency in its effect, polydatin action, can affect cellular growth and proliferation in HCC cancer cells in higher doses. This high dose-dependent effect, however, does not seemed to be focused on central glucose metabolism, but ROS accumulation and oxidative stress. Our results showed a close relationship between PPP inhibitor and reducing equivalents for antioxidant response which may show that this response is more dependent on NADPH from PPP activity, whereas glucose metabolism may depend more on NADH or NADPH from other pathways. With that being said, and based in our results, with also conclude the PPP inhibition is a therapeutical target with great potential for inhibition of cancer cell growth and proliferation and future studies should be conducted to unravel the full effect of this metabolic pathway inhibition further and better.

References

1. Sung H, Ferlay J, Siegal R, Laversanne M, Soerjomataram I, Jemal A, et al. Global cancer statistics 2020: GLOBOCAN estimates of incidence and mortality worldwide for 36 cancers in 185 countries. 2020 [cited 2021 Jul 16]. p. 1–2.
2. Sung H, Ferlay J, Siegel R, Laversanne. M, Soerjomataram I, Jemal A, et al. Cancer Tomorrow. 2020 [cited 2021 Jul 16]. p. 1.
3. WHO. Liver Cancer facts. 2020 [cited 2021 Jul 23]. p. 1–2.
4. Marengo A, Rosso C, Bugianesi E. Liver Cancer: Connections with Obesity, Fatty Liver, and Cirrhosis. Annual Review of Medicine. 2016 Jan 14;67(1):103–17.
5. Villanueva A. Hepatocellular Carcinoma. Longo DL, editor. New England Journal of Medicine. 2019 Apr 11;380(15):1450–62.
6. Wang M, Han J, Xing H, Zhang H, Li Z, Liang L, et al. Dysregulated fatty acid metabolism in hepatocellular carcinoma. Hepatic Oncology. 2016;3(4):241–51.
7. Karadag Soylu N. Update on Hepatocellular Carcinoma: A Brief Review from Pathologist Standpoint. Journal of Gastrointestinal Cancer. 2020 Dec 26;51(4):1176–86.
8. Marengo A, Rosso C, Bugianesi E. Liver Cancer: Connections with Obesity, Fatty Liver, and Cirrhosis. Annual Review of Medicine. 2016 Jan 14;67(1):103–17.
9. Gameiro PA. On The Reprogramming of the Krebs Cycle in Hypoxic and VHL-Deficient Cancer Cells. University of Coimbra; 2013.
10. Koppenol WH, Bounds PL, Dang C v. Otto Warburg's contributions to current concepts of cancer metabolism. Nature Reviews Cancer. 2011;11(5):325–37.
11. Ohshima K, Morii E. Metabolic reprogramming of cancer cells during tumor progression and metastasis. Vol. 11, Metabolites. 2021. p. 1–23.
12. Antico Arciuch VG, Elguero ME, Poderoso JJ, Carreras MC. Mitochondrial Regulation of Cell Cycle and Proliferation. Antioxidants & Redox Signaling. 2012 May 15;16(10):1150–80.
13. Bonuccelli G, Tsirigos A, Whitaker-Menezes D, Pavlides S, Pestell RG, Chiavarina B, et al. Ketones and lactate "fuel" tumor growth and metastasis. Cell Cycle. 2010 Sep 5;9(17):3506–14.
14. Yang M, Soga T, Pollard PJ, Adam J, Galluzzi L, Donato V, et al. The emerging role of fumarate as an oncometabolite. 2012.
15. Abrantes AM, Tavares LC, Pires S, Casalta-Lopes J, Mendes C, Simões M, et al. Metabolic effects of hypoxia in colorectal cancer by 13C NMR isotopomer analysis. BioMed Research International. 2014;2014.
16. Trepiana J, Meijide S, Navarro R, Hernández ML, Ruiz-Sanz JI, Ruiz-Larrea MB. Influence of oxygen partial pressure on the characteristics of human hepatocarcinoma cells. Redox Biology. 2017 Aug 1;12:103–13.
17. Guo R, Xu X, Lu Y, Xie X. Physiological oxygen tension reduces hepatocyte dedifferentiation in in vitro culture. 2017.
18. Kondo A, Yamamoto S, Nakaki R, Shimamura T, Hamakubo T, Sakai J, et al. Extracellular Acidic pH Activates the Sterol Regulatory Element-Binding Protein 2 to Promote Tumor Progression. Cell Reports. 2017 Feb 28;18(9):2228–42.
19. Patra KC, Hay N. The pentose phosphate pathway and cancer. Trends in Biochemical Sciences. 2014;39(8):347–54.
20. Ge T, Yang J, Zhou S, Wang Y, Li Y, Tong X. The Role of the Pentose Phosphate Pathway in Diabetes and Cancer. Frontiers in Endocrinology. 2020;11;1– 11.

21. Mele L, Paino F, Papaccio F, Regad T, Boocock D, Stiuso P, et al. A new inhibitor of glucose-6-phosphate dehydrogenase blocks pentose phosphate pathway and suppresses malignant proliferation and metastasis in vivo article. Cell Death and Disease. 2018;9(5).
22. Cox M, Nelson DL. Lehninger Principles of Biochemistry. 4 edition. SCHULTZ L, MORAN S, TONTONOZ M, editors. New York: W.H. Freeman; 2008. 1200 p.
23. Dentin R, Tomas-Cobos L, Foufelle F, Leopold J, Girard J, Postic C, et al. Glucose 6-phosphate, rather than xylulose 5-phosphate, is required for the activation of ChREBP in response to glucose in the liver. Journal of Hepatology. 2012;56(1):199–209.
24. Rajas F, Gautier-Stein A, Mithieux G. Glucose-6 phosphate, A central hub for liver carbohydrate metabolism. Metabolites. 2019;9(12):1–14.
25. Lu M, Lu L, Dong Q, Yu G, Chen J, Qin L, et al. Elevated G6PD expression contributes to migration and invasion of hepatocellular carcinoma cells by inducing epithelial-mesenchymal transition. Acta Biochimica et Biophysica Sinica. 2018 Apr 1;50(4):370–80.
26. Yalcin A, Telang S, Clem B, Chesney J. Regulation of glucose metabolism by 6-phosphofructo-2-kinase/fructose-2,6-bisphosphatases in cancer. Experimental and Molecular Pathology. 2009 Jun;86(3):174–9.
27. Du D, Liu C, Qin M, Zhang X, Xi T, Yuan S, et al. Metabolic dysregulation and emerging therapeutical targets for hepatocellular carcinoma. Acta Pharmaceutica Sinica B. 2022 Feb 1;12(2):558–80.
28. Inigo M, Deja S, Burgess SC. Ins and Outs of the TCA Cycle: The Central Role of Anaplerosis. Annual Review of Nutrition. 2021 Oct 11;41(1):19–47.
29. Ju HQ, Lin JF, Tian T, Xie D, Xu RH. NADPH homeostasis in cancer: functions, mechanisms and therapeutic implications. Signal Transduction and Targeted Therapy. 2020 Dec 7;5(1):231.
30. Stanton RC. Glucose-6-phosphate dehydrogenase, NADPH, and cell survival. IUBMB Life. 2012 May;64(5):362–9.
31. Belew GD, Silva J, Rito J, Tavares L, Viegas I, Teixeira J, et al. Transfer of glucose hydrogens via acetyl-CoA, malonyl-CoA, and NADPH to fatty acids during de novo lipogenesis. J Lipid Res. 2019;60(12):2050–6.
32. Lu YX, Ju HQ, Liu ZX, Chen DL, Wang Y, Zhao Q, et al. ME1 Regulates NADPH Homeostasis to Promote Gastric Cancer Growth and Metastasis. Cancer Research. 2018 Apr 15;78(8):1972–85.
33. Gameiro PA, Laviolette LA, Kelleher JK, Iliopoulos O, Stephanopoulos G. Cofactor balance by nicotinamide nucleotide transhydrogenase (NNT) coordinates reductive carboxylation and glucose catabolism in the tricarboxylic acid (TCA) cycle. Vol. 288, Journal of Biological Chemistry. 2013. p. 12967–77.
34. Metallo CM, Gameiro PA, Bell EL, Mattaini KR, Yang J, Hiller K, et al. Reductive glutamine metabolism by IDH1 mediates lipogenesis under hypoxia. Nature . 2012;481(7381):380–4.
35. Chen L, Zhang Z, Hoshino A, Zheng HD, Morley M, Arany Z, et al. NADPH production by the oxidative pentose-phosphate pathway supports folate metabolism. Nature Metabolism. 2019 Mar 1;1(3):404–15.
36. Fan J, Ye J, Kamphorst JJ, Shlomi T, Thompson CB, Rabinowitz JD. Quantitative flux analysis reveals folate-dependent NADPH production. 2014;
37. Zhang Z, TeSlaa T, Xu X, Zeng X, Yang L, Xing G, et al. Serine catabolism

generates liver NADPH and supports hepatic lipogenesis. Nature Metabolism. 2021 Dec 29 [cited 2022 Jul 3];3(12):1608–20.

38. Purcell EM, Torrey HC, Pound R v. Resonance Absorption by Nuclear Magnetic Moments in a Solid. Physical Review. 1946 Jan 1;69(1–2):37–8
39. Bloch F. Nuclear Induction. Physical Review. 1946 Oct 1;70(7–8):460–74.
40. Levitt MH. Spin dynamics: basics of nuclear magnetic resonance. Vol. 40, Magnetic Resonance in Chemistry. 2002.
41. Cheng J, Huang Y, Zhang X, Yu Y, Wu S, Jiao J, et al. TRIM21 and PHLDA3 negatively regulate the crosstalk between the PI3K/AKT pathway and PPP metabolism. Nature Communications. 2020 Dec 20 [cited 2022 Jun 29];11(1):1880.
42. Wiklund S. Multivariate Data Analysis for Omics. 2008.
43. Triba MN, le Moyec L, Amathieu R, Goossens C, Bouchemal N, Nahon P, et al. PLS/OPLS models in metabolomics: The impact of permutation of dataset rows on the K-fold cross-validation quality parameters. Vol. 11, Molecular BioSystems. Royal Society of Chemistry; 2015. p. 13–9.
44. Baskin KK, Nomura S, Wang Z, Karlstaedt A. Stable Isotopes for Tracing Cardiac Metabolism in Diseases. Frontiers in Cardiovascular Medicine.2021;8:734364.
45. Atta-ur-Rahman, Choudhary MI, Atia-tul-Wahab. Nuclear Overhauser Effect. In: Solving Problems with NMR Spectroscopy. Elsevier; 2016 [cited 2022 Jul 4]. p. 227–64.
46. Jin ES, Moreno KX, Wang JX, Fidelino L, Merritt ME, Sherry AD, et al. Metabolism of hyperpolarized [1-13 C]pyruvate through alternate pathways in rat liver. 2016;
47. Can E, Bastiaansen JAM, Couturier DL, Gruetter R, Yoshihara HAI, Comment A. [13C]bicarbonate labelled from hyperpolarized [1-13C]pyruvate is an in vivo marker of hepatic gluconeogenesis in fasted state. Communications Biology. 2022 Dec 10;5(1):10
48. Belew GD, di Nunzio G, Tavares L, Silva JG, Torres AN, Jones JG. Estimating pentose phosphate pathway activity from the analysis of hepatic glycogen ^{13} C-isotopomers derived from [U- ^{13} C]fructose and [U- ^{13} C]glucose. Magnetic Resonance in Medicine. 2020 Nov 17;84(5):2765–71.
49. Patrício JS, Dias-Pedroso D, Carvalho RA, Viera HLA, Jones JG. A simple method for quantifying de novo lipogenesis rate and substrate selection in cell cultures by ^{13} C NMR isotopomer analysis of the crude lipid fraction. NMR in Biomedicine. 2022 Mar;35(3).
50. Lane AN, Fan TWM, Higashi RM. Isotopomer-Based Metabolomic Analysis by NMR and Mass Spectrometry. Vol. 84, Methods in Cell Biology. 2008. p. 541–88.
51. World Health Organization. Standardization of procedures for the study of glucose-6-phosphate dehydrogenase : report of a WHO Scientific Group [meeting held in Geneva from 5 to 10 December 1966]. Geneva; 1967 [cited 2022 Jul 4].
52. Cohen P, Rosemeyer MA. Human Glucose-6-Phosphate Dehydrogenase: Purification of the Erythrocyte Enzyme and the Influence of Ions on its Activity. European Journal of Biochemistry. 1969 Mar;8(1):1–7.
53. Davis MI, Shen M, Simeonov A, Hall MD. Diaphorase Coupling Protocols for Red-Shifting Dehydrogenase Assays. ASSAY and Drug Development Technologies.

2016 Apr;14(3):207–12.
54. Carvalho RA, Rodrigues TB, Zhao P, Jeffrey FMH, Malloy CR, Sherry AD. A 13C isotopomer kinetic analysis of cardiac metabolism: Influence of altered cytosolic redox and [Ca2+]o. American Journal of Physiology - Heart and Circulatory Physiology. 2004 Aug [cited 2022 Jul 27];287(2 56-2):889–95.
55. Knowles BB, Howe CC, Aden DP. Human Hepatocellular Carcinoma Cell Lines Secrete the Major Plasma Proteins and Hepatitis B Surface Antigen. Science (1979). 1980 [cited 2022 Jul 18];209(4455):497–9.
56. van Wenum M, Adam AAA, van der Mark VA, Chang JC, Wildenberg ME, Hendriks EJ, et al. Oxygen drives hepatocyte differentiation and phenotype stability in liver cell lines. 2079;
57. Ferreira GK, Scaini G, Carvalho-Silva M, Gomes LM, Borges LS, Vieira JS, et al. Effect of l-Tyrosine In Vitro and In Vivo on Energy Metabolism Parameters in Brain and Liver of Young Rats. Neurotoxicity Research 2012 23:4. 2012 Jul 31 [cited 2022 Jul 19];23(4):327–35.
58. Meffert G, Gellerich FN, Margreiter R, Wyss M. Elevated creatine kinase activity in primary hepatocellular carcinoma. 2005.
59. Palde PB, Carroll KS. A universal entropy-driven mechanism for thioredoxin-target recognition.
60. Zhang J, Zhang B, Li X, Han X, Liu R, Fang J. Small molecule inhibitors of mammalian thioredoxin reductase as potential anticancer agents: An update. Medicinal Research Reviews. 2019 Jan 1;39(1):5–39.
61. Fang J, Luo L, Ke Z, Liu C, Yin L, Yao Y, et al. Polydatin protects against acute cholestatic liver injury in mice via the inhibition of oxidative stress and endoplasmic reticulum stress. Journal of Functional Foods. 2019 Apr 1;55:175–83.
62. Tang D, Zhang Q, Duan H, Ye X, Liu J, Peng W, et al. Review Article Polydatin: A Critical Promising Natural Agent for Liver Protection via Antioxidative Stress. 2022.
63. Parker AL, Kavallaris M, Mccarroll JA, Wymann MP. Microtubules and their role in cellular stress in cancer. 2014.
64. Kouda K, Iki M. Beneficial effects of mild stress (hormetic effects): dietary restriction and health. J Physiol Anthropol. 2010 [cited 2022 Jul 28];29(4):127–32.
65. Jiang X, Liu W, Deng J, Lan L, Xue X, Zhang C, et al. Polydatin protects cardiac function against burn injury by inhibiting sarcoplasmic reticulum Ca2+ leak by reducing oxidative modification of ryanodine receptors. Free Radical Biology and Medicine. 2013 Jul 1;60:292–9.
66. Huang K, Chen C, Hao J, Huang J, Wang S, Liu P, et al. Polydatin promotes Nrf2-ARE anti-oxidative pathway through activating Sirt1 to resist AGEs-induced upregulation of fibronetin and transforming growth factor-β1 in rat glomerular messangial cells. Molecular and Cellular Endocrinology. 2015 Jan 5;399:178–89.

~

Appendix

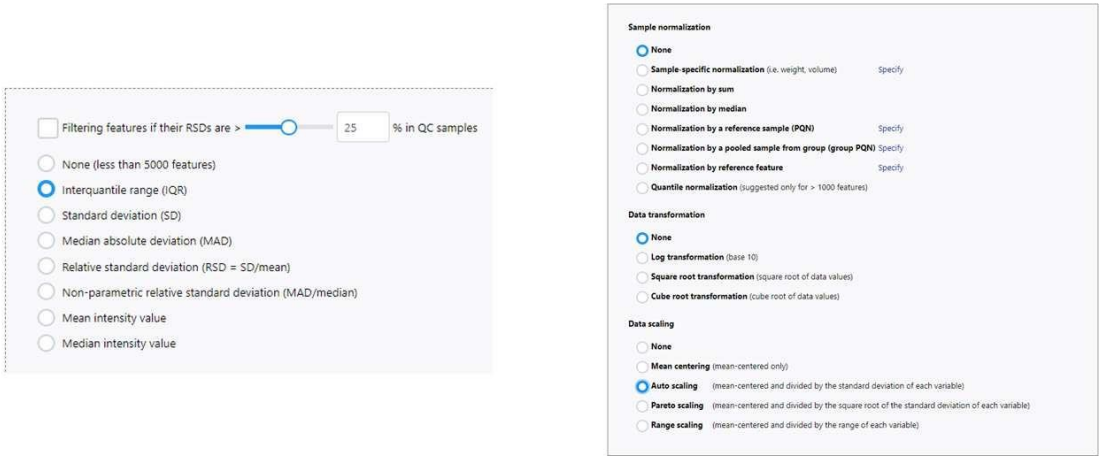

Figure 19 Processing parameters from MetaboAnalyst

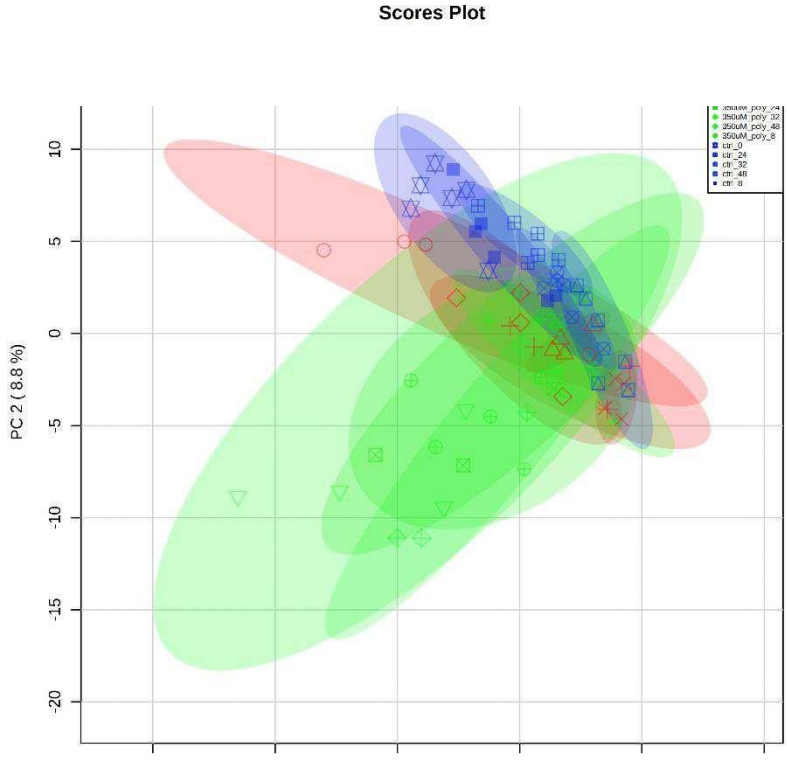

Figure 20 PCA for Control vs. 0.1 mM polydatin vs. 0.35 mM polydatin

PLS-DA cross validation details:

Measure	1 comps	2 comps	3 comps	4 comps	5 comps
Accuracy	0.075	0.15	0.2125	0.3	0.2625
R2	0.45827	0.67311	0.80424	0.89392	0.93619
Q2	0.13187	0.29275	0.32855	0.32489	0.27754

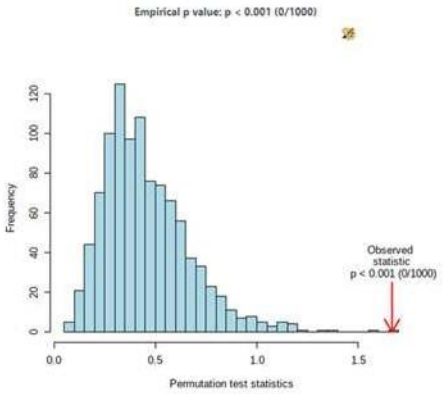

Figure 21 Quality parameters for the PLS-DA for Control vs. 0.1 mM of Polydatin vs. 0.35 mM Polydatin

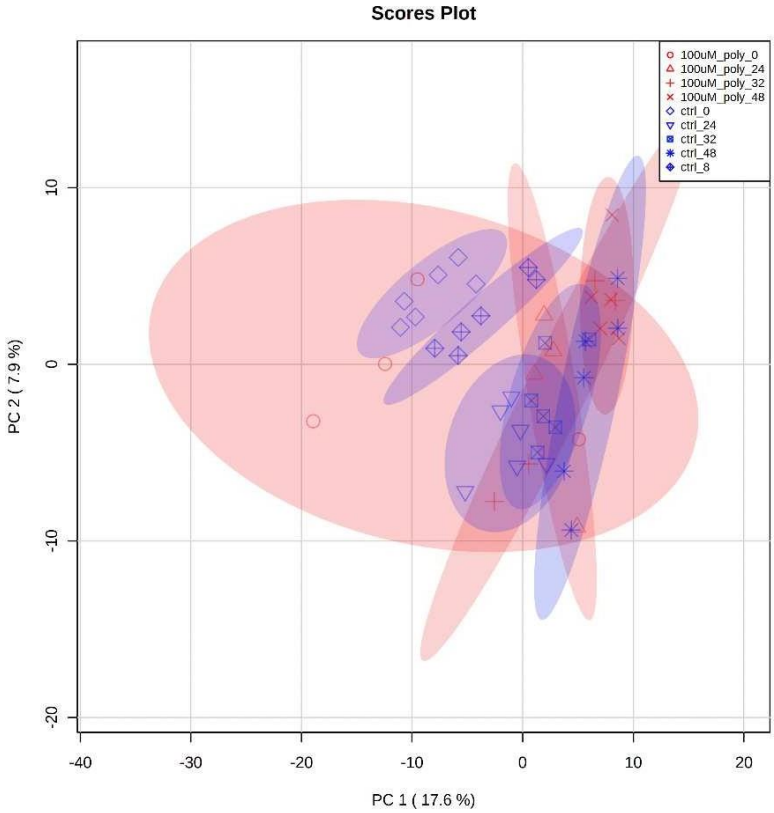

Figure 22 PCA for Control vs. 0.1 mM polydatin

PLS-DA cross validation details:

Measure	1 comps	2 comps	3 comps	4 comps	5 comps
Accuracy	0.1	0.21667	0.3	0.43333	0.41667
R2	0.54731	0.74241	0.89128	0.93217	0.97293
Q2	0.39842	0.46122	0.52719	0.5048	0.46642

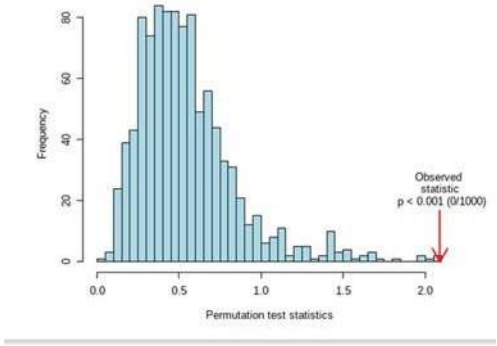

Figure 23 Quality parameters for the PLS-DA from Control vs. 100 µM of Polydatin

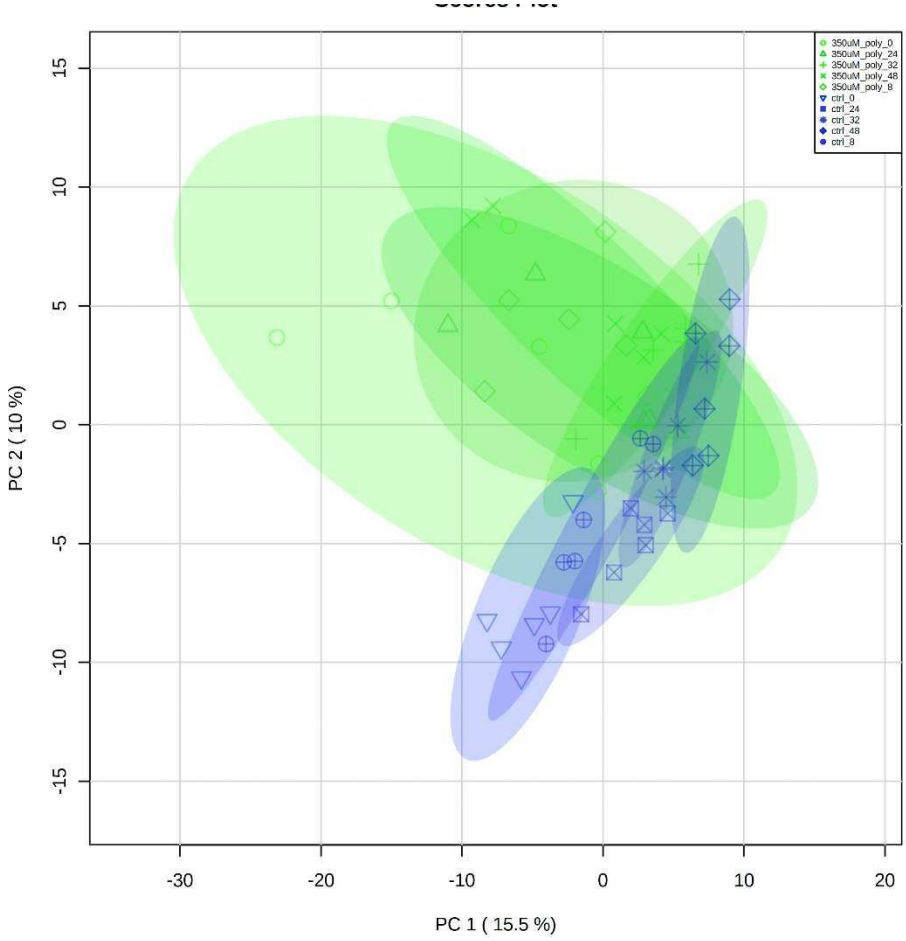

Figure 24 PCA for Control vs. 0.1 mM polydatin

PLS-DA cross validation details:

Measure	1 comps	2 comps	3 comps	4 comps	5 comps
Accuracy	0.12766	0.31915	0.29787	0.38298	0.40426
R2	0.6773	0.79776	0.94548	0.98142	0.99278
Q2	0.29609	0.41193	0.4273	0.38886	0.41212

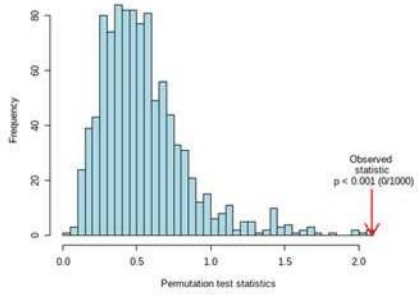

Figure 25 Quality parameters for the PLS-DA from Control vs. 350 µM Polydatin

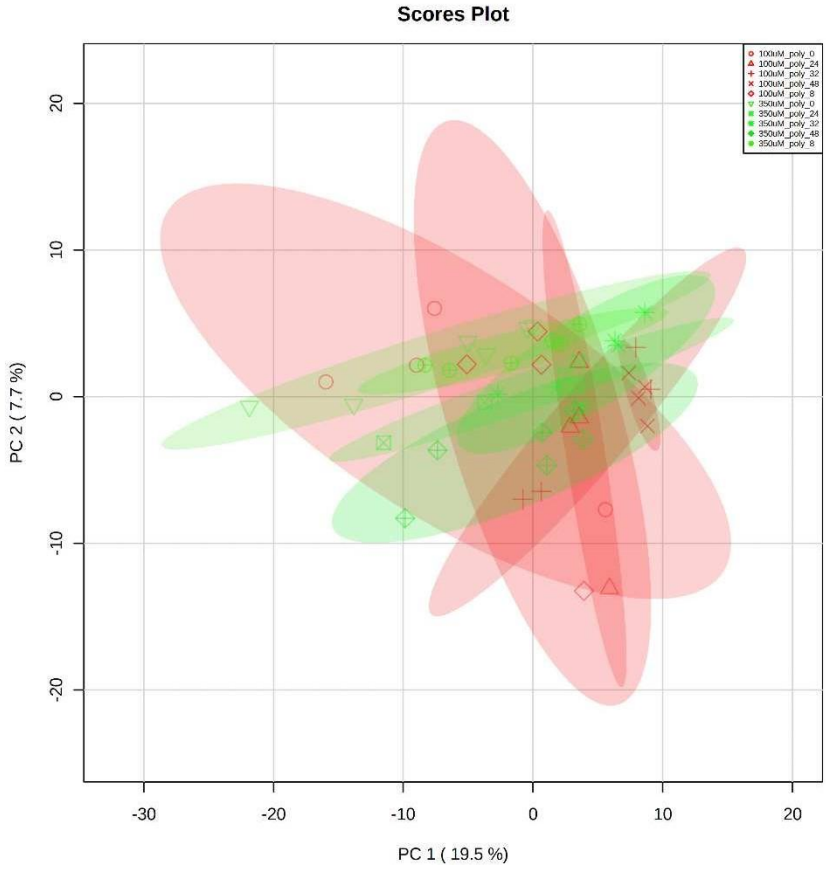

Figure 26 PCA for 0.1 mM polydatin vs 0.35 polydatin

PLS-DA cross validation details:

Measure	1 comps	2 comps	3 comps	4 comps	5 comps
Accuracy	0.1	0.21667	0.3	0.43333	0.41667
R2	0.54731	0.74241	0.89128	0.93217	0.97293
Q2	0.39842	0.46122	0.52719	0.5048	0.46642

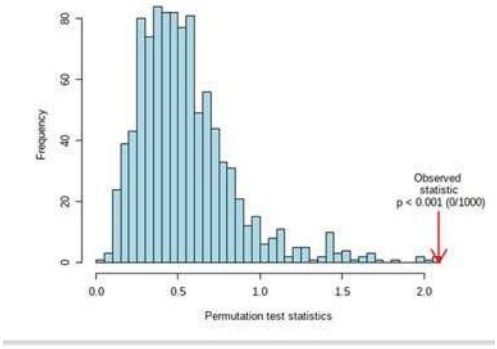

Figure 27 Quality parameters for the PLS-DA from Control vs. 100 µM of Polydatin

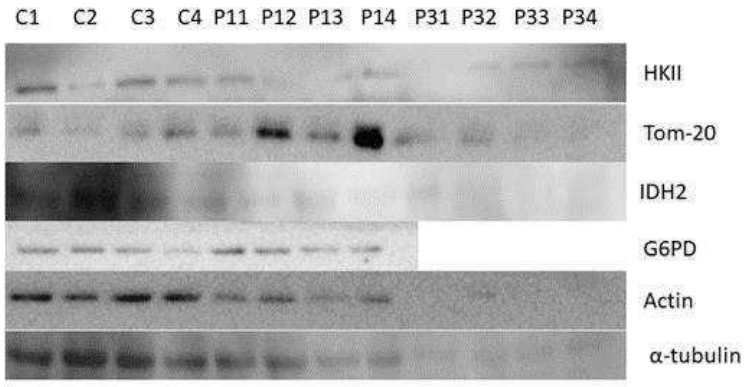

Figure 28 Western Blot bands for Hexokinase, Tom-20, Isocitrate dehydrogenase 2, Glucose-6-phosphate, Actin, and α-tubulin

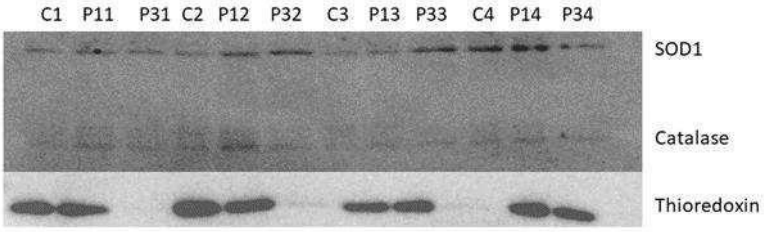

Figure 29 Western Blots bands for Superoxide dismutase 1, Catalase and Thioredoxin

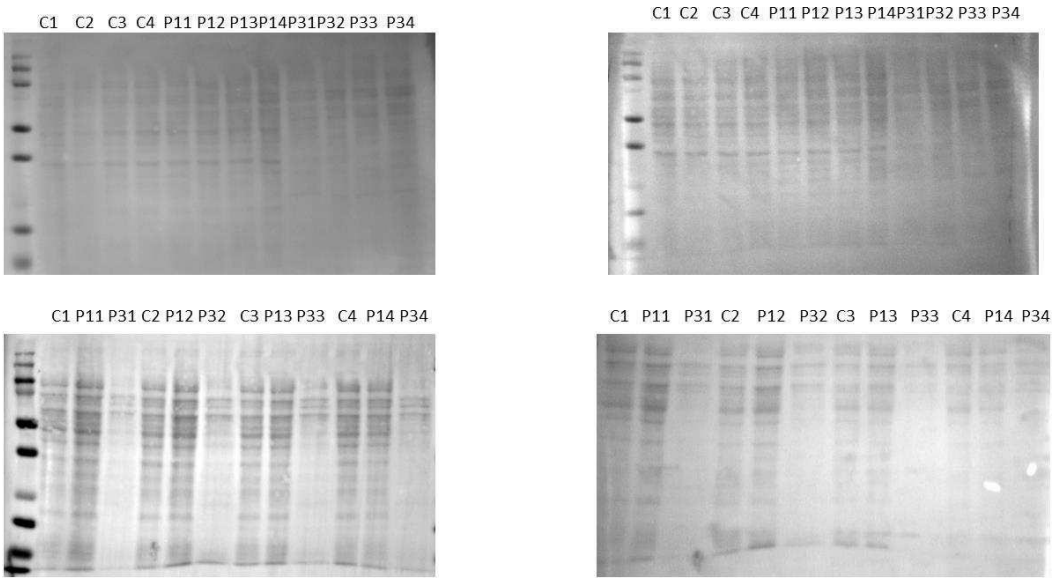

Figure 30 Representation from the gels coloured with Ponceau Red